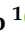# A Non-Invasive and Sustainable Characterization of Pigments in Wall Paintings: A Library of Apulian Colors

Giovanna Fioretti [1,*], Marina Clausi [1], Giacomo Eramo [1], Elisabetta Longo [2], Alessandro Monno [1], Daniela Pinto [1] and Gioacchino Tempesta [1]

[1] Earth and Geoenvironmental Sciences Department, University of Bari Aldo Moro, 70121 Bari, Italy
[2] Bega Restauri di Elisabetta Longo, 70013 Bari, Italy
[*] Correspondence: giovanna.fioretti@uniba.it

Abstract: This paper proposed a multianalytical, non-invasive, accessible and expensive (compared to traditional ones) approach for the characterization of pictorial surfaces. A set of 18 pigments and 37 mixtures widely used in the Middle Ages in the Apulia (Italy) artistic and archaeological contexts was considered, and corresponding replicas were produced. Pigments were first characterized by X-ray powder diffraction (XRPD), then replicas were studied by optical microscopy using a portable instrument, colorimetry and fiber optic reflectance spectroscopy (FORS). The investigation provided encouraging results, which allowed the creation of a library including diagnostic microscopic, colorimetric and reflectance markers of each pigment and the identification of the mixtures' components.

Keywords: portable microscope; FORS; colorimetry; pigments; wall paintings; database; Apulia

1. Introduction

The identification of pigments used in wall paintings is currently entrusted to the most modern and innovative analytical techniques, which provide fast and accurate results, even when portable analyses are performed directly on site. However, these techniques are not always available for economic reasons and require continuous and often expensive maintenance. All these methods have the significant advantage of being non-invasive, portable, practical, handy and space-saving, inexpensive and certainly provide quick and immediate data on the painting surfaces.

Even if the digital optical microscope was usually used only as a supporting tool for other analytical techniques, very noteworthy is the research presented by [1], who proposed an original processing protocol of images acquired by the digital microscope for the exhaustive characterization of paintings' surfaces.

Differently, fiber optic reflectance spectroscopy (FORS) was widely applied in the colored surface characterization field, i.e., for the identification of pigments used in pictorial retouching [2], in manuscripts [3] and in modern and contemporary paintings [4,5], for the analysis of red chalk drawing [6], historical glass deterioration [7], dyestuffs in artistic textiles [8] and in wall paintings of artistic and archaeological sites [9–11]. Besides, it appears very useful to detect color changes connected to aging, pigment alteration and the presence of alteration products [12]. In 2014, a very detailed database including FORS spectra of 54 historical pigments applied in different binders commonly used in artworks was presented [13]. Today there is still an open debate on the consideration of some parameters (pigment size, thickness of pictorial layer, pigment concentration in the binder, roughness of surface) on the reflectance pigments. Some authors [14–16] argue that these aspects determine a shift of the spectral features, verified on some pigments, others [17] that only a decrease in the reflectance intensity occurs, causing, at most, a flattening of the curve.

Moreover, the application of colorimetry for the measurements of chromatic coordinates, performed by a spectrophotocolorimeter, is commonly used as a preliminary characterization of pictorial surfaces, both in the case of single pigment and in the case of mixtures [18] and to distinguish different ochres on the basis of their colorimetric features [19]. Moreover, spectrophotocolorimetry was carried out for pigment identification [20], for characterization of graphic document alteration [21], and to create a reference library [22].

The approach proposed in this article aims to reduce the economic limits and to make fast, immediate and efficient investigations on pigments in situ. It is based on the combined use of portable digital optical microscopy, colorimetry and FORS. Considering some chromatic, dimensional and morphological parameters of pigment particles observed through the digital microscope and presented and discussed in the following paragraphs, it is possible to recognize pigments used in wall paintings. To verify the correct identification of pigments, microscopic characterization was compared with reflectance spectra obtained by means of FORS and colorimetric coordinates measured by the spectrophotocolorimeter. On the other hand, the presented results showed that the adopted methodological approach allows for the distinction of different pigments mixed in the same color. In fact, the custom of mixing different pigments to obtain a specific chromatic effect or to simulate a much more valuable and expensive pigment starting from cheaper and locally available raw materials is very common evidence in mural painting. Precisely by virtue of this phenomenon, to test the investigation protocol, experimental replicas of wall paintings were reproduced considering pigments and locally customary recipes, frequently found in artistic and archaeological contexts of Apulia covering a period of time from the 3rd century BC to the 16th century AD. In fact, in the region, previous archaeometric investigations of pictorial surfaces highlighted the recurrent use of common pigments, such as red and yellow ochres, green earth and carbon black and the custom of mixing these pigments to create different chromatic effects and to simulate more precious and expensive pigments. Among the most relevant research in this sense, the most representative were considered for this study. In particular, wall paintings in rupestrian sites [23–26], in churches [27–31] and in burial contexts [32] were taken into account as reference examples for the choice of pigments and mixtures to be used in replicas.

The final result was the creation of a library containing all the data of investigations carried out on the selected pigments, which could be considered a reference for the identification of pigments used in historical wall painting.

2. Materials

2.1. Experimental Replicas

For the preparation of experimental replicas, the workflow suggested by the tractate of Cennino Cennini [33] and followed in other experimental study cases [34,35] was considered, which in any case corresponds to the executive technique used in the regional wall paintings and adopted by restorers in the restoration of Apulian artworks. Locally available materials were chosen and as faithful as possible to the Apulian pictorial tradition and sample preparation was carried out following the traditional composition of the preparatory layers in the wall painting technique. Firstly, two bricks were recovered and thoroughly wetted before applying the subsequent preparation layers (Figure 1a). A layer of *arriccio* (about 20 mm thick) composed of hydraulic lime and aggregate, considering an aggregate:binder ratio of 3:1, was applied to the wet substrate (Figure 1b). The aggregate consisted of about 1/6 of fine grey river sand (0–2 mm), 1/6 of washed cocciopesto (2–3 mm), 1/3 of the fine rock powder (0–0.05 mm) and 1/3 of rock powder with larger grain size (0–2 mm). After the *arriccio* drying (about 10 days), the *intonaco* (plaster) layer (about 10 mm thick) was overlapped (Figure 1c). It consisted of local lime putty produced after a seasoning of 24 months and aggregate with an aggregate:binder ratio of 2:1. The aggregate was characterized by half of fine rock powder (0–0.05 mm) and half of coarser rock powder (0–2 mm). A preparatory outline was drawn on the still-wet plaster using the

traditional *cartone* technique and ochre, to obtain the track for pigment application. It was a grid consisting of 36 and 37 squares (3 × 3 cm) on the first and second support, respectively. Pigment layers were then applied on wet surfaces (Figure 1d) as described below.
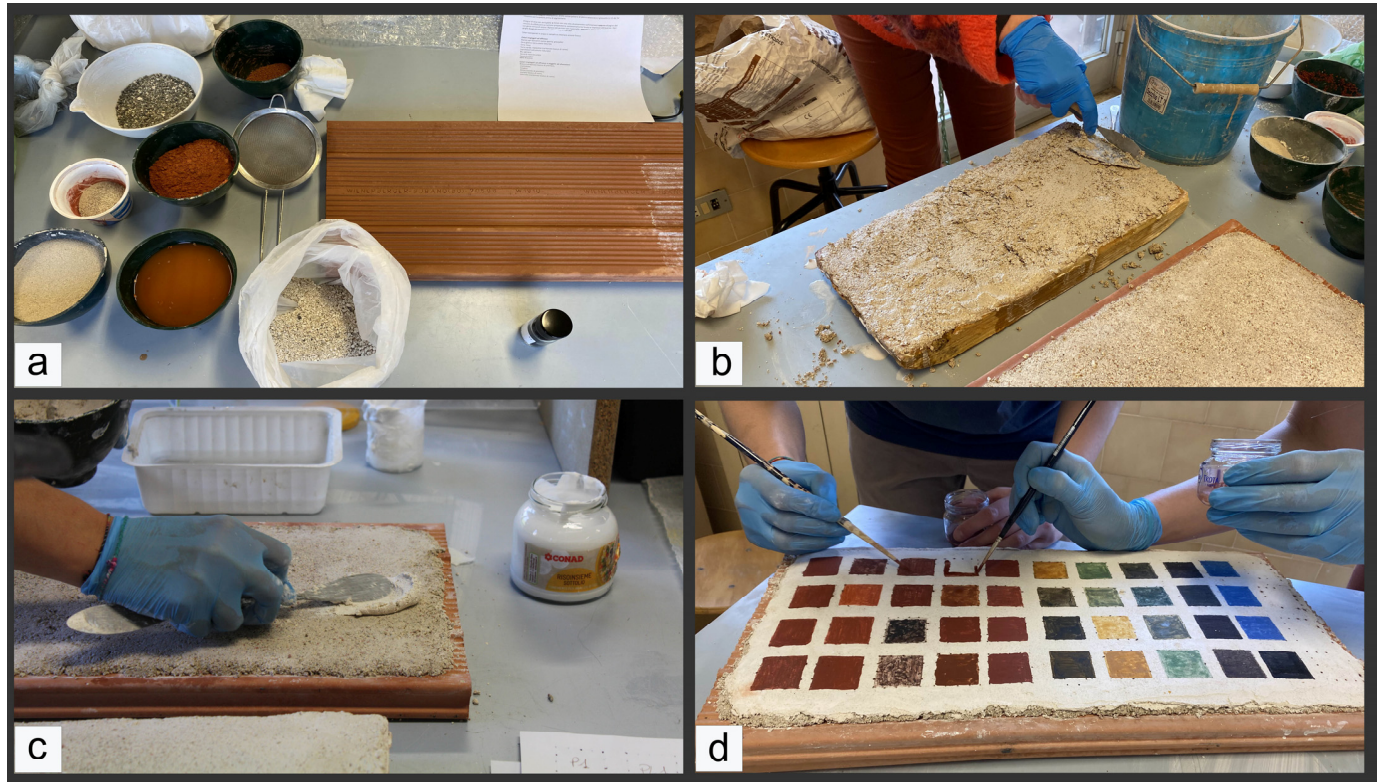

Figure 1. Preparation phases of replicas as follows: wetting of substratum (**a**), application of preparation layers (**b**), finishing layer (**c**) and painting (**d**).

2.2. Pigments and Mixtures

Pigments and recipes recurring in Apulian artistic heritage sites and therefore more representative of local wall painting, already discussed in the literature [23–32], were considered for the replica production and summarized in Tables 1 and 2. Precisely, 18 pigments, kindly offered by Kremer Pigmente GmbH & Co. KG (Aichstetten, Germany), were selected and applied both with the fresco and with the so-called *mezzo fresco* technique, which consists of mixing of pigment powder respectively in water and in lime [34,35]. Pigments were applied using the single layer application method and mixing 1 g of pigment with 1 mL of water, in case of fresco technique, and with 1 mL of lime, in case of *mezzo fresco* technique. We assumed that the thickness of the reproduced pictorial layers was comparable (30–150 μm) to each other to that verified in the local wall paintings because it is strictly connected to the "rule" of the painting technique, as also highlighted by the cited literature. Furthermore, starting from these materials, 21 pigment mixtures consisting of 1–5 pigments in different proportions were reproduced for a total of 37 different mixtures. They were placed on the still-wet plaster using the fresco technique, i.e., mixed with water, and in a single layer. The obtained replicas were left to dry for about twenty days before starting the analytical investigations. In the meantime, blackening and other chromatic changes due to the interaction with the environment (specific humidity and sunlight exposition) and with lime occurred (details for each color transformation were reported in Section 4.2.1).

Table 1. Sample names and preliminary information) on selected pigments used to paint all the 36 replicas (18 by frescos technique and 18 by lime painting technique). The chemical composition and the grain size of pigments were provided by Kremer Pigmente GmbH & Co. KG.

Color	Samples		Pigment	Kremer Code	Grain Size	Chemical Composition
	Frescos	Lime Painting				
Red	P01	PL01	Hematite	48651	1.25 ± 0.15 μm	Fe_2O_3
	P02	PL02	Red ochre	11273	0–80 μm	-
	P03	PL03	Minium	42500	-	Pb_3O_4
	P04	PL04	Cinnabar	10625	20–50 μm	HgS
	P05	PL05	Realgar	10800	175 μm	As_4S_4
Yellow	P06	PL06	Yellow ochre	11272	0–80 μm	-
	P07	PL07	Massicot	43010	8–11 μm	PbO
Green	P08	PL08	Green earth	11010	0–80 μm	$K(MgFe^{3+})(Si_4O_{10})(OH)_2$
	P09	PL09	Malachite	10300	0–120 μm	$CuCO_3 \cdot Cu(OH)_2$
	P10	PL10	Verdigris	44450	-	$C_4H_6CuO_4 \cdot H_2O$, $Cu(CH_3COO)_2 \cdot [Cu(OH)_2]_3 \cdot 2H_2O$
Blue	P11	PL11	Azurite	10200	0–120 μm	$2CuCO_3 \cdot Cu(OH)_2$
	P12	PL12	Egyptian blue	10060	< 120 μm	$CaCuSi_4O_{10}$
	P13	PL13	Lapis lazuli	10520	-	$(Na,Ca)_8[(SO_4,S,Cl)_2(AlSiO_4)_6]$
Brown	P14	PL14	Brown earth	11620	-	-
Black	P15	PL15	Bone black	47100	50–300 μm	C
	P16	PL16	Vine black	47000	<70 μm (max. 15–50)	C
	P17	PL17	Ivory black	12000	~10 μm	C
White	P18	PL18	Bianco San Giovanni	11415	<150 μm	$Ca(OH)_2$

Table 2. Color, mixed pigments and find sites (with references) of each mixture. In the columns of pigments, in brackets, percentages of each of them were reported. Proportion of pigments was chosen by the authors starting from the qualitative description of recipes reported in the considered literature. For some recipes other additional proportions were considered.

Sample	Color	Pigments				Site	References
MR1	Red	Hematite (70)	Cinnabar (10)	Minium (10)	Realgar (10)	St. Maria Veterana church, 9th–15th century, Triggiano (Bari)	[27]
MR2a	Red	Red ochre (75)	Hematite (25)			Festoni Tomb, 3rd–2nd century BC, Taranto	[32]
MR2b		Red ochre (50)	Hematite (50)				
MR2c		Red ochre (25)	Hematite (75)				
MR3a	Red	Hematite (75)	Minium (25)			St. Matteo all'Arena Hypogeum, 12th–13th century, Monopoli (Bari)	[24]
MR3b		Hematite (50)	Minium (50)				
MR3c		Hematite (25)	Minium (75)				
MR4a	Dark red	Red ochre (75)	Vine black (25)			St. Angelo in cryptis cave, 11th–16th century, Santeramo in Colle (Bari)	[25]
MR4b		Red ochre (50)	Vine black (50)				
MR4c		Red ochre (25)	Vine black (75)				

Table 2. *Cont.*

Sample	Color	Pigments			Site	References
MR5a		Red ochre (75)	Brown earth (25)			
MR5b	Dark red	Red ochre (50)	Brown earth (50)		Gonfalone crypt, 9th–16th century, Tricase (Lecce)	[26]
MR5c		Red ochre (25)	Brown earth (75)			
MR6a		Red ochre (75)	Yellow ochre (25)			
MR6b	Orange	Red ochre (50)	Yellow ochre (50)		St. Maria Veterana church, 9th–15th century, Triggiano (Bari)	[27]
MR6c		Red ochre (25)	Yellow ochre (75)			
MR7a		Hematite (75)	Bianco San Giovanni (25)			
MR7b	Pink	Hematite (50)	Bianco San Giovanni (50)		St. Maria Veterana church, 9th–15th century, Triggiano (Bari)	[27]
MR7c		Hematite (25)	Bianco San Giovanni (75)			
MR8	Pink	BiancoSan Giovanni (50)	Hematite (30)	Yellow ochre (20)	St. Maria Veterana church, 9th–15th century, Triggiano (Bari)	[27]
MY1a		Yellow ochre (75)	Vine black (25)			
MY1b	Yellow-brown	Yellow ochre (50)	Vine black (50)		St. Angelo in cryptis cave, 11th–16th century, Santeramo in Colle (Bari)	[25]
MY1c		Yellow ochre (25)	Vine black (75)			
MY2a		Yellow ochre (75)	Massicot (25)		St. Maria Veterana church, 9th–15th century, Triggiano (Bari); Santi Stefani crypt at Vaste, 11th–16th century, Lecce; Santa Maria delle Cerrate, 12th–13th century, Lecce	
MY2b	Yellow	Yellow ochre (50)	Massicot (50)			[27,30,31]
MY2c		Yellow ochre (25)	Massicot (75)			
MG1a		Green earth (75)	Malachite (25)			
MG1b	Dark green	Green earth (50)	Malachite (50)		Gonfalone crypt, 9th–16th century, Tricase (Lecce)	[26]
MG1c		Green earth (25)	Malachite (75)			
MG2	Green	Green earth (90)	Egyptian blue (10)		Festoni Tomb, 3rd–2nd century BC, Taranto	[32]
MG3	Green	Green earth (50)	Verdigris (40)	Vine black (10)	St. Maria Veterana church, 9th–15th century, Triggiano (Bari)	[27]
MBG1	Blue-grey	Vine black (50)	Bianco San Giovanni (30)	Yellow ochre (20)	Seppannibale temple, 10th–11th century, Fasano (Bari); St. Maria Veterana church, 9th–15th century, Triggiano (Bari)	[27–29]

Table 2. *Cont.*

Sample	Color	Pigments				Site	References
MBG2	Blue-grey	Vine black (40)	Bianco San Giovanni (30)	Yellow ochre (10)	Red ochre (10)	St. Angelo in cryptis cave, 11th–16th century, Santeramo in Colle (Bari); Festoni Tomb, 3rd–2nd century BC, Taranto	[25,32]
MBG3	Blue-grey	Bone black (40)	Bianco San Giovanni (30)	Yellow ochre (10)	Red ochre (10)	St. Maria Veterana church, 9th–15th century, Triggiano (Bari)	[27]
MB1	Black-brown	Vine black (50)	Yellow ochre (30)	Green earth (20)		St. Maria Veterana church, 9th–15th century, Triggiano (Bari)	[27]
MB2	Black-blue	Vine black (90)	Red ochre (10)			Santi Stefani crypt at Vaste, 11th–16th century, Lecce	[31]
MB3	Black-blue	Bone black (90)	Red ochre (10)			Santi Stefani crypt at Vaste, 11th–16th century, Lecce	[31]

3. Analysis Methods

Although suitable technical data sheets were provided by the manufacturer company, all the pigments were characterized from a mineralogical point of view through X-ray powder diffraction (XRPD). The core of the adopted analytical approach consisted of the comparison between features of pigments observed under the digital microscope, their colorimetric coordinates highlighted by a spectrophotocolorimeter and their spectral features measured by means of fiber optic reflectance spectroscopy. The microscopic observation involved all 73 samples (18 pigments with water, 18 pigments with lime and 37 mixtures), whereas only the preserved or less changed colors were studied from a colorimetric point of view.

3.1. X-ray Power Diffraction (XRPD)

A PANalytical Empyrean diffractometer equipped with a Real-Time Multiple Strip (RTMS) PIXcel3D detector and Cu-Kα radiation was used for the mineralogical characterization of pigments. Analytical conditions were the following: 40 mA and 40 kV, 2θ range from 3 to 70°, virtual scan of 0.026°2θ, counting time 60 s per step. X-ray patterns were analyzed using the software X'Pert High Score 3.0e, which includes the ICSD database.

3.2. Portable Digital Microscopy

The used portable digital microscope was a very light and extremely handy instrument, as it was just over 10 cm in length. It consisted of Dino-Lite Edge Digital Microscope AM7915MZT equipped with a 5-megapixel resolution sensor, an automatic magnification reading (10–220×) and a polarizer; the lighting was due to 8 switchable LEDs with an infrared filter (>650 nm). The presence of extended depth of field and extended dynamic range systems allowed us to take satisfying and focused images.

Under the digital microscope, chromatic, morphological, optical and other parameters concerning single particles of pigments and their relationship with the background were considered specified as follows: the first parameters were texture (unimodal or multimodal) and size of the most frequent pigment particle if they were distinguishable at 220× magnification. The second type of marker concerned a qualitative evaluation of color with the naked eye and specific hue (red, orange, yellow, green, cyan, blue, purple, magenta, white, black, chosen for their large distribution in paintings), saturation (high, medium, low) and brightness (high, medium, low). After, morphological characteristics, namely, shape, rounding (rounded, mixed, angular), gloss (high, medium, low), edge (sharp, thick, soft) and appearance (intact, mixed, fractured), were examined.

3.3. Spectrophotocolorimetry

Colorimetric analysis was performed by Konica Minolta CM-2600d portable spectrophotocolorimeter, under the D65 standard illuminant, with an aperture mask with a diameter of 6 mm and a standard observer at a 10° angle. The instrument works in the wavelength range from 360 to 740 nm with a wavelength step size of 10 nm. It was previously calibrated using zero and white calibration provided by the instrument manufacturer. The spectrocolorimeter measured each point three times and then returned three sets of colorimetric data in the CIEL*a*b* system, represented by the three values of L* (brightness), a* (green-red axis) and b* (blue-yellow axis) [36]. For each set of coordinates, mean and standard deviation were calculated (reported in the Supplementary Materials).

3.4. Fiber Optic Reflectance Spectroscopy

FORS analysis was carried out with a custom system by Avantes. The AvaSpec-ULS2048XL- USB2 model spectrophotometer and an AvaLight-HAL-S tungsten halogen light source were combined with a reflection probe FCR-7UV200-2-ME UV/VIS. The spectrophotometer used works from 200 to 1100 nm with a spectral resolution of about 1.4 nm. The spectra were recorded from 300 to 900 nm because of noise in UV and IR regions. The diameter of the probe, about 200 μm, allows taking measurements even of very small painted areas depending on the distance from the surface. The capability to collect a reflectance spectrum from a small area was an important feature to avoid inhomogeneous colored areas, especially when the surface was damaged or fractured with the tampering of the time. Diffuse reflectance spectra of the samples were referenced against the WS-2 reference tile, guaranteed to be reflective at 98% or more in the spectral range investigated. The FORS spectra of all the painted replicas, with a spot size of about 2 mm in diameter, were acquired on the parchment. In all measurements, the distance between the probe and the sample was fixed (~5 mm). The instrumental parameters were as follows: 400 ms integration time and 10 scans for a total acquisition time of 4 s for each spectrum. The spectra were collected with Avasoft 8.0 and then exported in Spectragryph® [37] for visualization and comparison with standards.

4. Results and Discussion

4.1. Mineralogical Analysis of Pigment Powders

The mineralogical composition of pigments is reported in Table 3. XRPD patterns showed a multi-crystalline composition for the majority of pigments.

Hematite and red ochre pigments, belonging to the reds group, showed hematite and illite as common crystalline phases, with further traces of dolomite in the former (hematite) and quartz, feldspars and gypsum minerals in the latter (red ochre). It is worth noting that the occurrence of accessory phases such as aluminosilicates, quartz, anatase or carbonates in red ochre is common; however, it may affect the color [38].

XRPD confirmed the phase purity of the minium pigment, while lead sulfide (galena) was found in cinnabar, in addition to the main HgS phase.

Realgar pigment showed the following different As-bearing mineral phases: realgar, orpiment, dimorphite and alacranite. The concurrent presence of different arsenic sulfides in red and yellow pigments is well-known and widely investigated [39].

Yellow ochre consisted of a mixture of the iron hydroxide goethite and other minerals, such as quartz, calcite, gypsum and chlorite. A similar composition was found in the pigment characterization performed by [40]. Similarly, the massicot spectrum included the lead oxide mineral (massicot) and other minerals, among which chalcopyrite and pyrophyllite.

Green earth was a mixture of different minerals such as celadonite, phillipsite, montmorillonite and calcite. Verdigris pigment contained the crystalline phases of copper acetate hydrate and quartz, while in malachite, the pigment of the copper mineral malachite together with quartz and orthoferrosilite was found.

Table 3. Mineralogical composition of pigments and PDF numbers of mineralogical phases.

Pigment	Mineralogical Phases
Hematite	**hematite** [1] (Fe_2O_3); **dolomite** [2] ($CaMg(CO_3)_2$); **illite** [3] ($Al_4H_{12}KO_{18}Si_8$)
Red ochre	**hematite** [4] (Fe_2O_3); **quartz** [5] (SiO_2); **gypsum** [6] ($CaSO_4 \cdot 2H_2O$); **illite** [7] ($Al_4H_{12}KO_{18}Si_8$); **potassium feldspar** [8] ($KAlSi_3O_8$)
Minium	**minium** [9] (Pb_3O_4)
Cinnabar	**cinnabar** [10] (HgS); **galena** [11] (PbS)
Realgar	**realgar** [12] (As_4S_4); **alacranite** [13] (AsS); **orpiment** [14] (As_2S_3); **dimorphite** [15] (As_4S_3); **quartz** [16] (SiO_2); **cristobalite** [17] (SiO_2)
Yellow ochre	**goethite** [18] ($FeO(OH)$); **quartz** [19] (SiO_2); **gypsum** [20] ($CaSO_4 \cdot 2H_2O$); **calcite** [21] ($CaCO_3$); **chlorite** [22]
Massicot	**massicot** [23] (PbO); **chalcopyrite** [24] ($CuFeS_2$); **bindheimite** [25] ($Pb_2Sb_2O_6$ (O,OH)); **pyrophyllite** [26] ($Al_2Si_4O_{10}(OH)_2$)
Green earth	**calcite** [27] ($CaCO_3$); **celadonite** [28] ($K(MgFe^{3+})(Si_4O_{10})(OH)_2$); **phillipsite** [29] ($KCa(Si_5Al_3)O_{16} \cdot 6H_2O$); **montmorillonite** [30]
Malachite	**malachite** [31] ($Cu_2CO_3 \cdot (OH)_2$); **quartz** [32] (SiO_2); **orthoferrosilite** [33] ($FeSiO_3$)
Verdigris	**copper acetate hydrate** [34] (($CH_3COO)_2Cu \cdot H_2O$); **quartz** [35] (SiO_2)
Azurite	**azurite** [36] ($Cu_3(CO_3)_2 \cdot (OH)_2$); **quartz** [37] ($SiO_2$); **kaolinite** [38] ($Al_2(Si_2O_5)(OH)_4$); **muscovite** [39]
Egyptian blue	**cuprorivaite** [40] ($CaCuSi_4O_{10}$);
Lapis lazuli	**lazurite** [41] ($Na_6Ca_2Al_6Si_6O_{24}$ ($SO_4)_2$); **wollastonite** [42] ($CaSiO_3$); **biotite** [43] ($K(Mg, Fe^{+2})3(Al, Fe^{+3})Si_3O_{10}$ (OH, F)$_2$; **sodalite** [44] ($Na_8Si_6Al_6O_{24}Cl_2$)
Brown earth	**hematite** [45] (Fe_2O_3); **goethite** [46] ($FeO(OH)$); **oehmite** [47] ($AlO(OH)$); **anatase** [48] (TiO_2); **cristobalite** [49] (SiO_2)
Ivory black	**hydroxyapatite** [50] (Ca_{10} ($PO_4)_6(OH)_2$); **whitlockite** [51] ($Ca_3(PO_4)_2$)
Bianco di S. Giovanni	**calcite** [52] ($CaCO_3$); **portlandite** [53] ($CaOH_2$)

1: PDF 01-072-0469; 2: PDF 01-075-1759; 3: PDF 00-035-0652; 4: PDF# 33-0664; 5:PDF# 79-1906; 6: PDF# 33-0311; 7: PDF# 26-0911; 8: PDF# 71-1544; 9: PDF 00-041-1493; 10: PDF 01-080-2192; 11: PDF 00-005-0592; 12: PDF 00-041-1494; 13: PDF 00-025-0057; 14: PDF 00-024-0075; 15: PDF 00-026-0126; 16: PDF 01-083-0539; 17: PDF 01-075-1544; 18: PDF 00-001-0401; 19: PDF 01-079-1910; 20: PDF 01-070-0984; 21: PDF 01-083-0578; 22: PDF 01-0 07-1082; 23: PDF 00-038-1477; 24: PDF 00-037-0471; 25: PDF 00-018-0687; 26: PDF 01-071-1051; 27: PDF 01-083-0578; 28: PDF 01-083-2008; 29: PDF 01-039-1375; 30: PDF 01-013-0135; 31: PDF 00-041-1390; 32: PDF 01-085-0404; 33: PDF 01-083-0667; 34: PDF 00-027-0145; 35: PDF 01-079-1915; 36: PDF 00-072-0539; 37: PDF 00-078-2315; 38: PDF 01-080-0886; 39: PDF 00-007-0042; 40: PDF# 85-0158; 41: PDF 00-044-1396; 42: PDF 00-027-0088; 43: PDF 01-083-1366; 44: PDF 01-072-0029; 45: PDF 00-033-0664; 46: PDF 00-029-0713; 47: PDF 01-076-1871; 48: PDF 00-021-1272; 49: PDF 01-075-1544; 50: PDF 01-074-0566; 51: PDF 01-070-1786; 52: PDF 00-047-1743; 53: PDF 01-072-0156.

Among blue pigments, azurite shows the presence of azurite, quartz, kaolinite and muscovite minerals. Egyptian blue X-ray diffraction pattern showed solely cuprorivaite peaks, whereas lapis lazuli consisted of the mineral lazurite, which is the main responsible for the blue color, along with different accessory minerals including wollastonite, biotite and sodalite, as well known in literature [41–43].

Brown earth diffractogram showed peaks of hematite, goethite, boehmite, anatase and cristobalite.

XRPD spectrum of ivory black comprised an amorphous hump in which the peaks related to the following two calcium phosphate minerals were recognized: hydroxyapatite, a crystalline non-carbon constituent, considered the main clue for the identification of the pigment [44] and whitlockite.

Bianco San Giovanni pigment showed the crystalline phases of portlandite and calcite, the latter formed upon reaction with ambient CO_2, in agreement with X-ray analysis performed on the same pigment by [45].

4.2. Microscopic Observation

4.2.1. Pure Pigments Replicas

As a premise, it is necessary to state that the parameters examined for the characterization were observed by microscope both in pigments applied with water and in the pigments mixed with lime. No substantial differences in the considered parameters between the two painting techniques were observed, the reason why only P samples, i.e., those used by the fresco technique, will be considered in this paragraph.

Moreover, after the painting of replicas, some pigments showed a different coloration from that indicated in the technical sheets, therefore a new grouping was made, moving P10 (verdigris) into the blue group, P14 (brown earth) into the red group and creating a separate group of orange pigments including P03 (minium) and P05 (realgar).

A summary of observation by digital portable microscope was reported in Table 4 and an atlas of photomicrographs of every pigment was available in Supplementary Material (Figures S1–S17).

In the group of reds, hematite and red ochre (Figure 2a), despite being two very similar pigments both from a chromatic point of view and because of the same chromophore iron oxides [19,38,46], under the microscope, they appeared clearly distinguishable. P01 (hematite) showed a unimodal texture, given by an extremely fine and not visible dark red pigment (at magnifications lower than 220×, considering the instrumental conditions of the microscope); P02 (red ochre) showed a very dark red color and a bimodal texture given by a finer and invisible fraction and the other of about 25 μm with a compact shape, rounded edges and opaque appearance. Conversely, cinnabar [47–49] (Figure 2b) appeared extremely different as follows: sample P04 showed unimodal texture and was composed of pigment particles of about 20 μm, characterized by a massive shape but with angular edges, high gloss and very thick edges. Furthermore, the microscope revealed that pigment started its blackening process connected to several mechanisms, among which interaction with different chemical species when specific humidity and sunlight exposition occur [43–45].

Brown earth [38–46] showed a bimodal distribution due to a finer and not visible fraction together with larger (20 μm), massive, rounded particles of a dark red pigment with low saturation, brightness and gloss of color.

In the orange color group, P03, consisting of minium [50], was a very saturated and bright orange color composed of a very fine fraction and, therefore, not visible at the instrument magnification. In realgar [39] of sample P05 (Figure 2c), the microscopic observation highlighted the presence of a portion of photo-degraded particles [51] where is well still visible the original pigment. It consisted of the following two types of particles: the first was characterized by a saturated and intense yellow color, larger in size (about 100 μm), with edges both sharp and thick; the second was marked by a saturated and bright red color, smaller (50 μm), with sharp edges. Both showed prismatic shapes, angular edges and high gloss.

Yellow pigments were yellow ochre [19,38,46] and massicot [50]. In P06 (yellow ochre, Figure 2d), the microscopic observation revealed a bimodal texture due to a very fine and invisible fraction and particles of about 30 μm, yellow in color with low saturation and brightness, massive and angular, with low gloss, sharp edges and intact appearance. P07 (massicot), although partially altered [52], differed for unimodal texture, very limited size (<10 μm), a highly saturated and bright yellow color, massive shapes and mixed rounding, medium gloss; edge appeared soft and appearance seemed to be intact.

The two green analyzed pigments, green earth and malachite [53], appeared extremely different and easily recognizable under the microscope. In fact, sample P08 of green earth exhibited bimodal distribution due to an invisible very fine fraction and a coarser portion (35 μm) composed of a green, massive and rounded particle with a sharp edge and intact aspect. In P09 (malachite, Figure 2e), very saturated and bright green particles (50 μm), marked by elongated shape, soft edge and fractured aspect, were observed.

The blue group included verdigris, azurite, Egyptian blue and lapis lazuli [53–56]. Sample P10 (verdigris, Figure 2f) showed a bimodal texture composed on the one hand of

cyan and acicular particles (60 µm) and, on the other hand, of blue, massive and rounded particles (80 µm), these last marked by thick edges. Sample P11 (azurite), as expected, turned black in color but by means of a digital microscope, blue, prismatic with angular edges particles were recognized. Besides, these showed a typical fractured aspect. Sample P12 (Egyptian blue, Figure 2g) displayed a larger size (60 µm) and a very saturated and bright blue; in this case, the pigment particles appeared massive in shape, both rounder and angular, with sharp edges. Different appeared sample P13 (lapis lazuli, Figure 2h), which showed opaquer color, finer size (10 µm) and tabular shape.

Referring to the black pigments [57], the microscopic observation revealed that P15 (bone black) was composed of very fine particles that were not visible but that create a uniform black-grey background. P16 (vine black) consisted of black and fine (10 µm) particles, marked by tabular shape. Differently, P17 (ivory black) had a larger size (30 µm) and a massive shape. Both showed soft edges.

The identification of P18 (bianco San Giovanni) was very limited because it was applied on a white substratum. However, the observation of distinctive parameters was easier if pigment was mixed with other pigments, the reason why their selection was carried out by observing replicas MR7, MR8, MB5, MBG1, MBG2 and MBG3. The white pigment showed unimodal texture, size of about 80 µm, spherical shape, rounded and sharp edge and intact aspect.

Observation of replicas under the digital microscope was conducted also using the polarizing light, as reported in Table 4. In this case, the observations did not produce different results, as the pigments showed the same features both with and without the light polarizer. In general, a moderate lowering of the gloss was observed, which led to a better visibility of the pigment particles (Figure 3). The only exceptions concerned the marked lowering of the gloss in P8 (cinnabar) and P12 (Egyptian blue) and the increase in chromatic saturation in P9 (malachite) and P10 (verdigris). Furthermore, for P15 (bone black), P16 (vine black) and P17 (ivory black) there was a lowering of saturation and brightness.

Table 4. A summary of observation by digital portable microscope, reporting distinctive parameters of each pigment. n.v.: not visible.

Color	Pigment	Sample	Texture	D Moda	Color								Morfology			
					Unpolarised Light				Polarised Light							
					Hue	Saturation	Brightness	Gloss	Hue	Saturation	Brightness	Gloss	Shape	Rounding	Edge	Appearence
Red	Hematite	P01	unimodal	n.v.	red	medium	medium	n.v.	red	medium	medium	n.v.	n.v.	n.v.	n.v.	n.v.
	Red ochre	P02	bimodal	25 µm	red	medium-low	low	low	red	medium-low	low	low	massive	rounded	sharp	intact
				n.v.	red	medium-low	low	n.v.	red	medium-low	low	n.v.	n.v.	n.v.	n.v.	n.v.
	Cinnabar	P04	unimodal	20 µm	magenta	high	medium	high	magenta	high	medium	low	massive	angular	thick	mixed
	Brown earth	P14	bimodal	20 µm	red	low	low	low	red	low	low	low	massive	rounded	sharp	intact
				n.v.	red	low	low	low	red	low	low	low	massive	rounded	sharp, thick	intact
Orange	Minium	P03	unimodal	n.v.	orange	high	high	n.v.	orange	high	high	n.v.	n.v.	n.v.	n.v.	n.v.
	Realgar	P05	bimodal	100 µm	yellow	high	high	high	yellow	high	high	high	prismatic	angular	sharp, thick	intact
				50 µm	red	high	high	high	red	high	high	high	prismatic	angular	sharp	mixed
Yellow	Yellow ochre	P06	bimodal	n.v.	yellow	low	low	n.v.	yellow	low	low	n.v.	n.v.	n.v.	n.v.	n.v.
				30 µm	yellow	low	low	low	yellow	low	low	low	massive	rounded	sharp	intact
	Massicot	P07	unimodal	10 µm	yellow	high	high	medium	yellow	high	high	medium	massive	mixed	soft	intact
Green	Green earth	P08	bimodal	n.v.	green	low	medium	n.v.	green	low	low	n.v.	n.v.	n.v.	n.v.	n.v.
				35 µm	green	low	low	low	green	low	low	low	massive	rounded	sharp	intact
	Malachite	P09	unimodal	50 µm	green	medium-high	high	high	green	high	high	high	elongated	angular	soft	fractured
Blue	Verdigris	P10	bimodal	60 µm	cyan	high	high	medium	cyan	high	high	medium	acicular	angular	soft	intact
				80 µm	blue	high	high	medium	blue	high	high	medium	massive	rounded	thick	intact
	Lapis lazuli	P11	unimodal	15 µm	blue	high	medium-high	medium	blue	high	medium-high	medium	prismatic	angular	sharp	fractured
	Egyptian blue	P12	unimodal	60 µm	blue	high	high	high	blue	high	high	low	massive	mixed	sharp	intact
	Lazurite	P13	unimodal	10 µm	blue	high	medium-high	low	blue	high	medium-high	low	tabular	mixed	sharp	intact

Table 4. *Cont*.

Color	Pigment	Sample	Texture	D Moda	Color								Morfology			
					Unpolarised Light				Polarised Light							
					Hue	Saturation	Brightness	Gloss	Hue	Saturation	Brightness	Gloss	Shape	Rounding	Edge	Appearence
Black	Bone black	P15	unimodal	n.v.	black	medium	medium-high	medium	black	low	low	low	n.v.	n.v.	n.v.	n.v.
	Vine black	P16	unimodal	10 μm	black	medium	medium-high	high	black	low	low	low	tabular	angular	soft	intact
	Ivory black	P17	unimodal	30 μm	black	medium	medium	medium	black	low	low	low	massive	rounded	soft	intact
White	Bianco San Giovanni	MR7, MR8, MBG1, MBG2, MBG3	unimodal	80 μm	white	n.v.	n.v.	n.v.	white	n.v.	n.v.	n.v.	spherical	rounded	sharp	intact
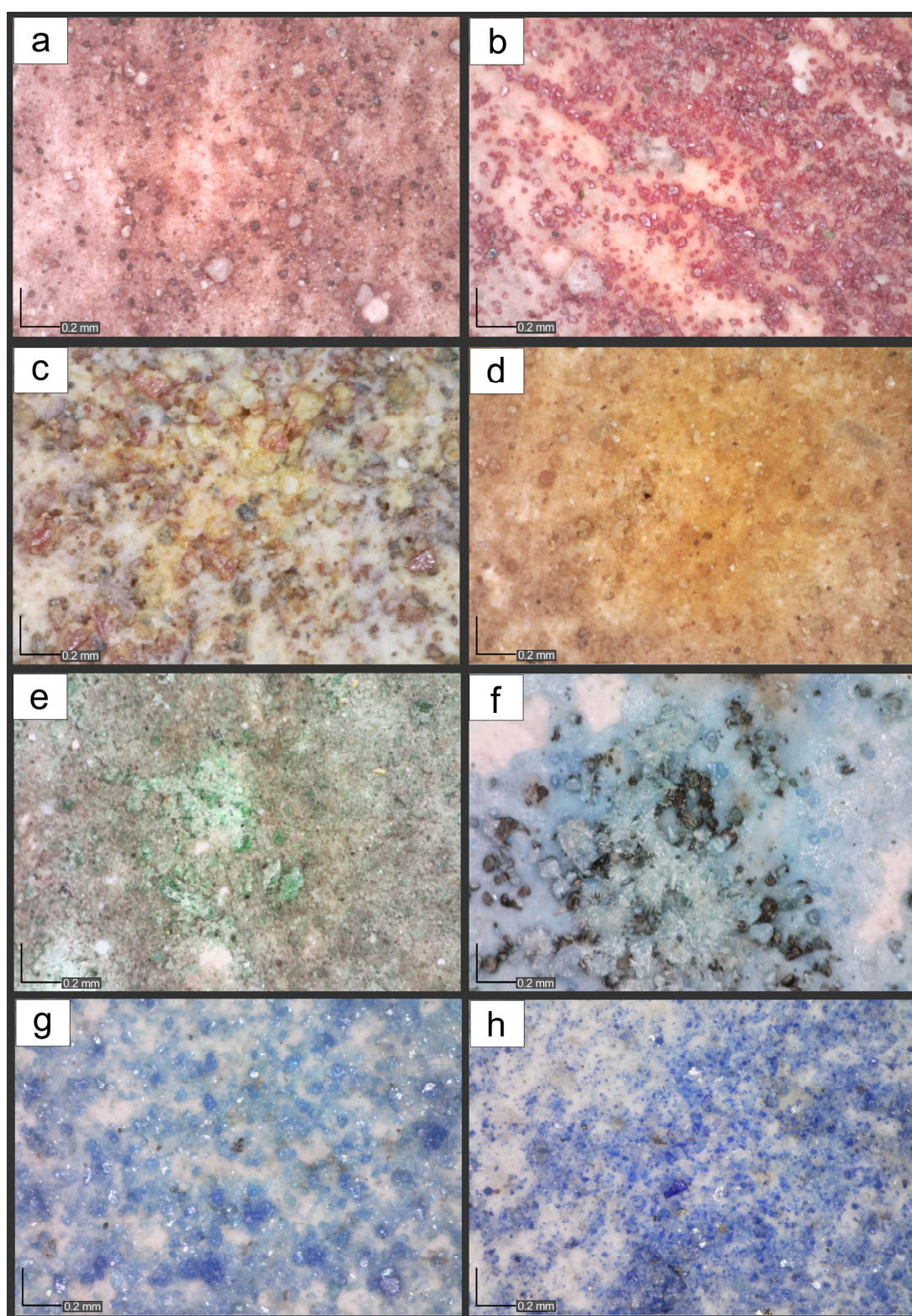
Figure 2. Photomicrographs of some replicas painted with the following pure pigments: P02, *Red ochre* (**a**); P04, cinnabar (**b**); P05, realgar (**c**); P06, yellow ochre (**d**); P09, malachite (**e**); P10, verdigris (**f**); P12, egyptian blue (**g**); P13, lapis lazuli (**h**).

4.2.2. Mixtures Replicas

In replicas of pigment mixtures, pigment characteristics observed under the digital microscope were compared with the parameters of each individual pigment reported in Table 4. Although the composition of the mixtures was known, this comparison allowed the identification of every single pigment in almost all replicas. The proportions referred to in the following paragraph are shown in Table 3.

In the MR1 sample (Figure 3a; hematite, cinnabar, minium, realgar), a red background was composed of an extremely fine hematite, within which magenta-red particles (20 μm) of cinnabar with thick edges, globular shape and high gloss could be clearly distinguished. Realgar and minium were not visible even if a yellow pigment (probably the yellow fraction of realgar) was glimpsed.

The MR2 replica, obtained by mixing hematite and red ochre in three proportions (a, b, c), showed an intense red background color given by a fine and invisible pigment comparable to hematite and dark red spherical particles (25 μm) with opaque appearance referable instead to the coarser fraction of red ochre. In the three variants, the latter increased as the percentage of red ochre increased.

The MR3 sample, composed of hematite and minium in three proportions (a, b, c), presented a red background, which turned to orange in the variant with the highest amount of minium. No pigment particles were discernible.

In the replicas of the MR4 group composed of red ochre and vine black (in three different proportions a, b, c), under the polarizer microscope, an opaque and very dark red ochre (20 μm) with a rounded shape could be clearly distinguished from vine black, which had elongated shape and fine grain size (10 μm). Under non-polarized light, the latter had a very high gloss.

The MR5 sample, consisting of red ochre and brown earth in the three proportions (a, b, c), was characterized by dark red background, given by the finer fraction of red ochre, and contained two different pigments. These last appeared under the microscope very similar in shape and size (20–25 μm) but differed in the edges, which in red ochre were sharp and in brown earth were thick, and in the color, brownish in the first and reddish in the second.

A very similar condition was found in the MR6 group, composed of red ochre and yellow ochre in the three proportions (a, b, c). Indeed, results revealed two types of visible pigment, which were very similar in size and shape, and differed in color (dark red and golden yellow). The background color acquired more red or yellow hues in relation to the increase in red ochre or yellow ochre amounts, respectively.

In the three replicas (a, b, c) of MR7 (Figure 3b), a very intense and saturated red background was due to the hematite, in which the bianco San Giovanni pigment composed of rounded and white particles with dimensions between 40 and 90 μm was dispersed.

The microscope observations of the MR8 sample highlighted characteristics matching the previous sample, but with the addition of yellow particles of approximately 25 μm in size, referable to yellow ochre.

The samples of the MY1 group (Figure 3c) clearly showed the presence of yellow ochre, consisting of particles of about 25 μm, opaque and rounded, mixed with a very fine (10 μm) vine black pigment marked to elongated shape and extremely high gloss under the non-polarized light of the microscope.

In the case of the MY2 replicas, results disclosed yellow ochre characterized by a bimodal texture, including a fine fraction responsible for the background yellow color and coarser particles (20 μm) with globular shape. No traces of massicot were visible.
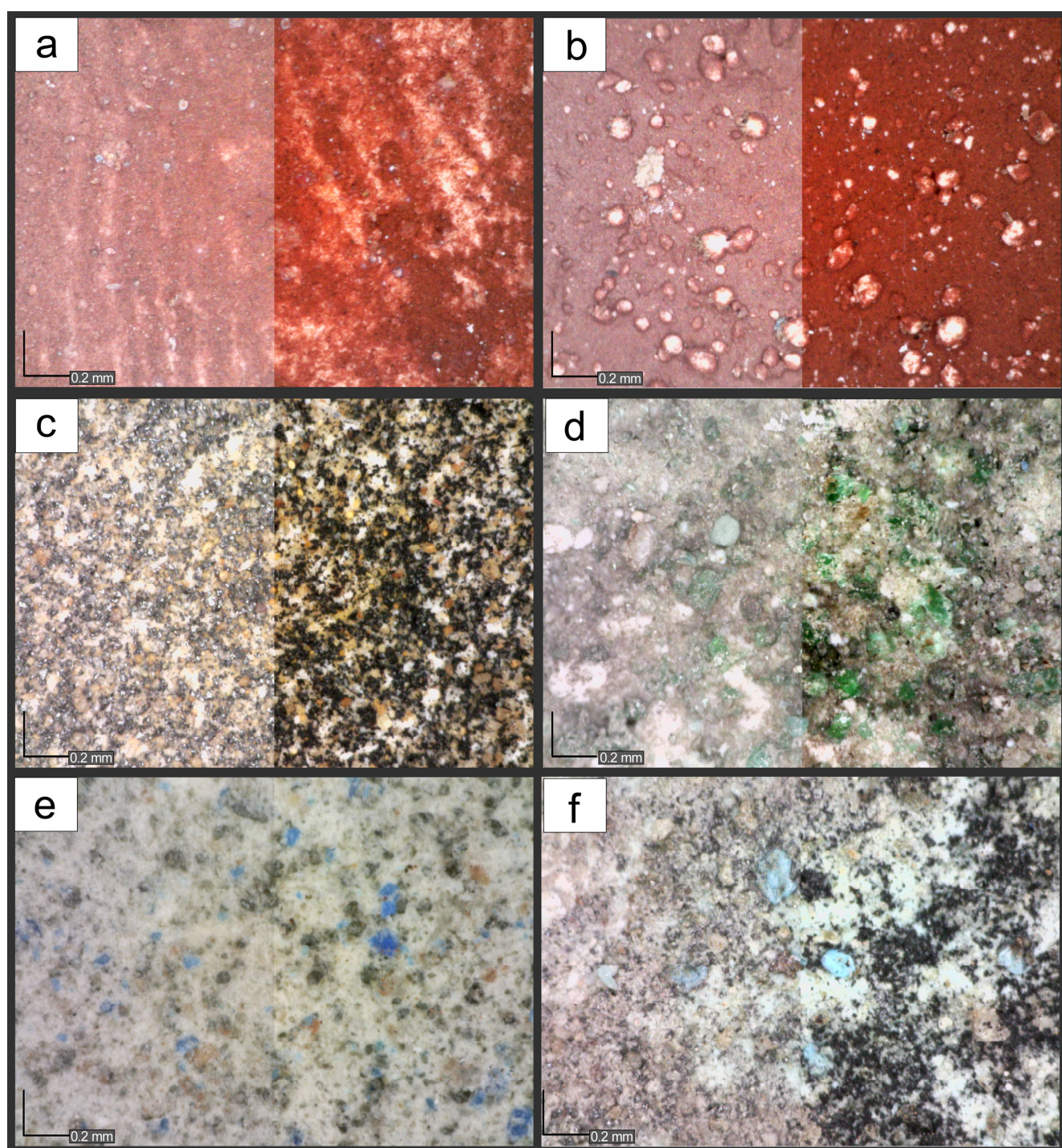
Figure 3. Photomicrographs, with (on the **right**) and without (on the **left**) light polariser, of significant replicas painted with the following mixtures of pigments: MR1 (**a**), MR7a (**b**), MY1b (**c**), MG1a (**d**), MG2 (**e**) and MG3 (**f**).

The results relating to samples MG1a, MG1b and MG1c (Figure 3d), composed of green earth and malachite, revealed the presence of the following two clearly different pigments: the first was greyish green, scarcely saturated and bright, with rounded shape and size of about 40–50 μm; the second showed saturated and bright color, very angular edges and fractured appearance and sizes comparable to the previous one. The described features were emphasized under the polarized light of the microscope.

A similar case was in the MG2 group (Figure 3e), where a variable amount of Egyptian blue was mixed together with green earth; the blue pigment was characterized by a distinctive, very saturated and bright blue color, globular shape and dimensions of about 60–65 μm.

In the MG3 replica (Figure 3f), consisting of a mixture of green earth, verdigris and vine black, the three pigments can be clearly distinguished. The first, composed of rounded particles of green-grey color and about 45 μm in size; the second given by cyan-colored particles, massive shape, angular edges and size, between 75 and 90 μm; the third, characterized by black particles, elongated shape, size around 10 μm, high gloss under non-polarized light.

In the MBG1 replica, vine black, bianco San Giovanni and yellow ochre were clearly distinguished under the microscope as follows: a predominant black pigment characterized by elongated shape, size of about 10 μm and high gloss in which a roundish white pigment of variable dimensions between 50 and 100 μm and a yellow and opaque pigment, with rounded shape and size of about 30–40 μm were mixed.

Similarly, the MBG2 sample showed the same features as the previous one except for the addition of red ochre, which displays dark color, rounded edges, massive shape and size of 30 μm.

MBG3 showed the same composition as MBG2 but with different markers of black pigment. In the latter, in fact, the pigment particles were not visible under the microscope and had a low gloss by virtue of the replacement of vine black with bone black.

A very comparable situation occurred in MB2 and MB3 samples composed of vine black and red ochre and bone black and red ochre, respectively. In both cases, the red ochre was well identifiable by its chromatic and morphological characteristics. The vine black of the MB2 sample showed the typical elongated shape, dimensions of about 10 μm, and high gloss, while the bone black of the MB3 sample was so fine that it was invisible and did not show significant gloss.

4.3. Color Coordinates

4.3.1. Pure Pigments Replicas

The colorimetric L*a*b* coordinates are reported in the Supplementary Material. The a* and b* coordinates are plotted for pure pigments applied by fresco (round indicator) and lime painting (triangle indicator) techniques in the graph in Figure 4.

Regarding the red colors, the graph shows that red ochre and hematite had comparable values of a* and b*, both in the case of frescos and lime paintings. Instead, cinnabar deviated towards higher values of b. Realgar displayed lower values of b* and higher values of a*. Minium appeared as an outlier since was characterized by higher values of a* and b*. Referring to the two yellow analyzed pigments, a significant difference in the two coordinates was evident because in the yellow ochre, the values of b* were superior, and conversely, in the massicot they were closer to 0, although a* values remained comparable. Brown earth showed values of a* and b* quite close to those of hematite and red ochre.
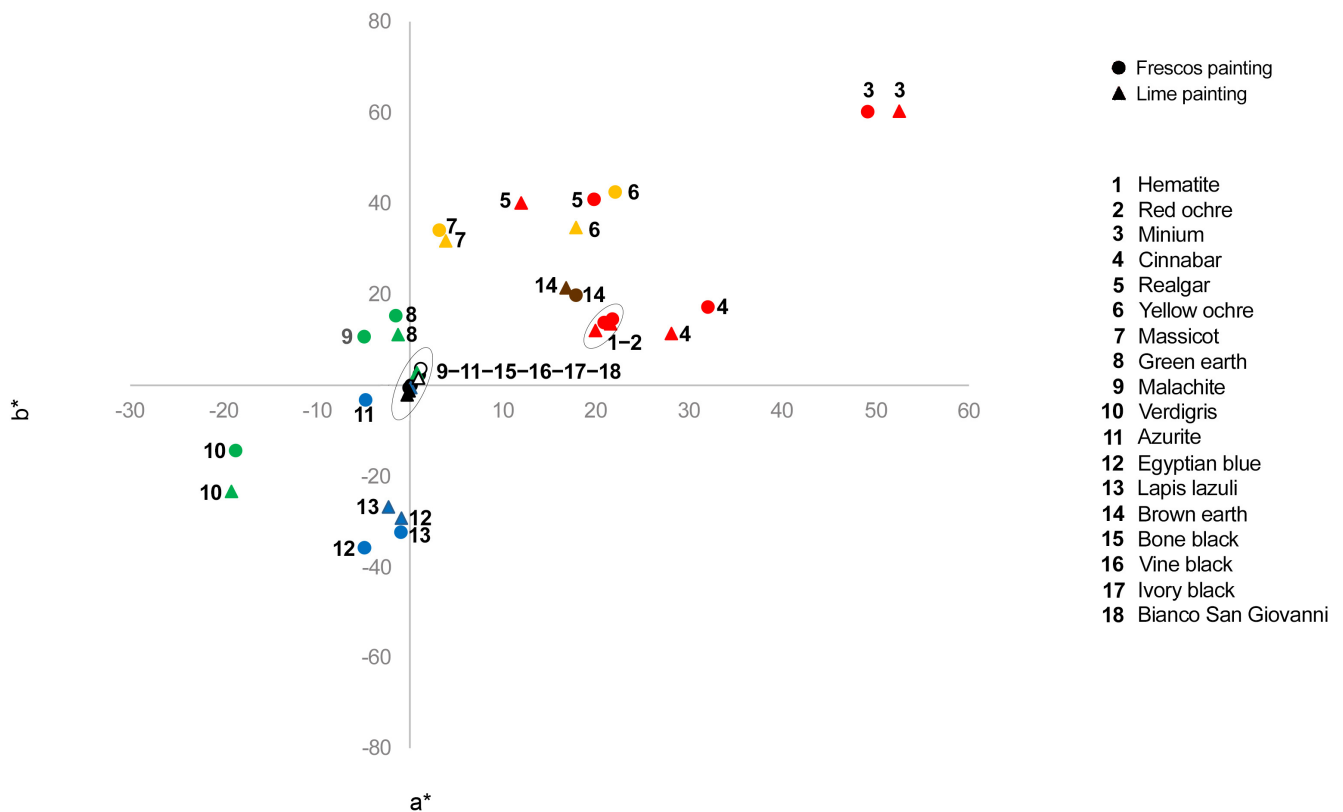
Figure 4. Biplot of a* and b* values of CIEL*a*b* coordinates measured on pigments applied by frescos (circle) and lime painting (triangle) techniques.

As concerns blue pigments, Egyptian blue and lapis lazuli displayed clearly negative and very close coordinates, in particular in the case of Egyptian blue applied with lime and lapis lazuli applied with water.

Different was the case of azurite, where the colorimetry revealed values of a* and b* equal to 0 due to the blackening occurring in the lime painting technique. For this reason, also malachite, mixed with lime, showed the same values; as regards the other greens, the green earth had positive but very low values of a* and negative values of b*, while the verdigris presented very low values of both coordinates.

The values of a* and b* of the three black pigments (vine, bone and ivory blacks) and bianco San Giovanni were equal to 0 and were comparable to the malachite and blue pigments applied with lime.

Furthermore, the interpretation of colorimetric data suggested that there was an appreciable chromatic difference between the two painting techniques. In almost all cases, the values of a* and b* coordinates (Figure 4) for each pigment dissolved in water and in lime were close; however, distinguishable. Moreover, in the graph in Figure 5, the variation of the L* coordinate was shown in pigments applied with water and those applied with lime. It pointed out that these values were very close for red and yellow pigments, and on the contrary, in the case of blue, green, brown and black pigments, the coordinate differed more significantly. In the latter case, the only exception was given by the vine black, where the L* values of the pigment applied in frescos and, when applied in lime painting, were matching.
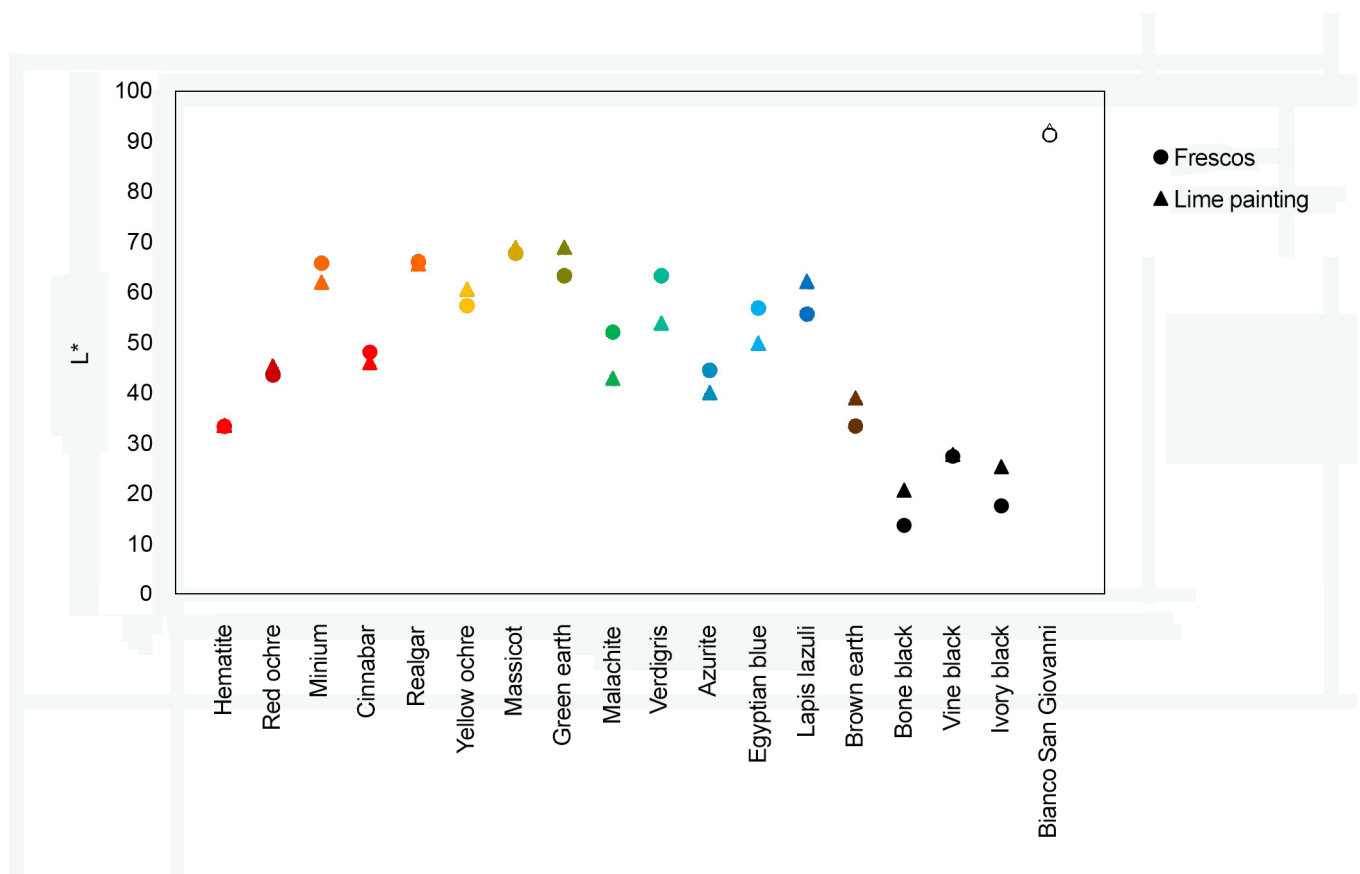
Figure 5. Plot showing variation of L* coordinate in pigments applied with water (circle) and those applied with lime (triangle).

4.3.2. Mixtures Replicas

The colorimetric data of the pigment mixtures (reported in Supplementary Material) are represented in the graph in Figure 6. Points appeared rather scattered and were positioned in areas belonging to the predominant pigments of the mix. However, a significant linear correlation ($R^2 = 0.9956$) was observed in the case of MR1, MR2 (a, b, c), MR3 (a, b, c), MR7 (a, b, c) and MR8 (Figure 7).

In these samples, the a* coordinate ranged from 22.88 to 35.01, and the b* coordinate ranged from 15.46 to 19.73, with an outlier at 30.57. All these samples corresponded to the mixtures containing hematite. The percentage of hematite ranged from 25 to 75 wt.%.

4.4. Reflectance Fingerprint

4.4.1. Pure Pigments Replicas

Outputs of fiber optic reflectance spectroscopy were spectra, which represented the reflectance fingerprint of each examined pigment. A first consideration concerns the similarity between the spectra of pigment applied with water (fresco technique) and pigment applied with lime (*mezzo fresco* technique). In this last case, spectra showed a slight variation of reflectance values; however, the spectral features were centered at the same wavelength. For this reason, we consider only the spectra of the first group. The main reflectance spectral features and the spectra were reported in Table 5 and Figure 8, respectively.
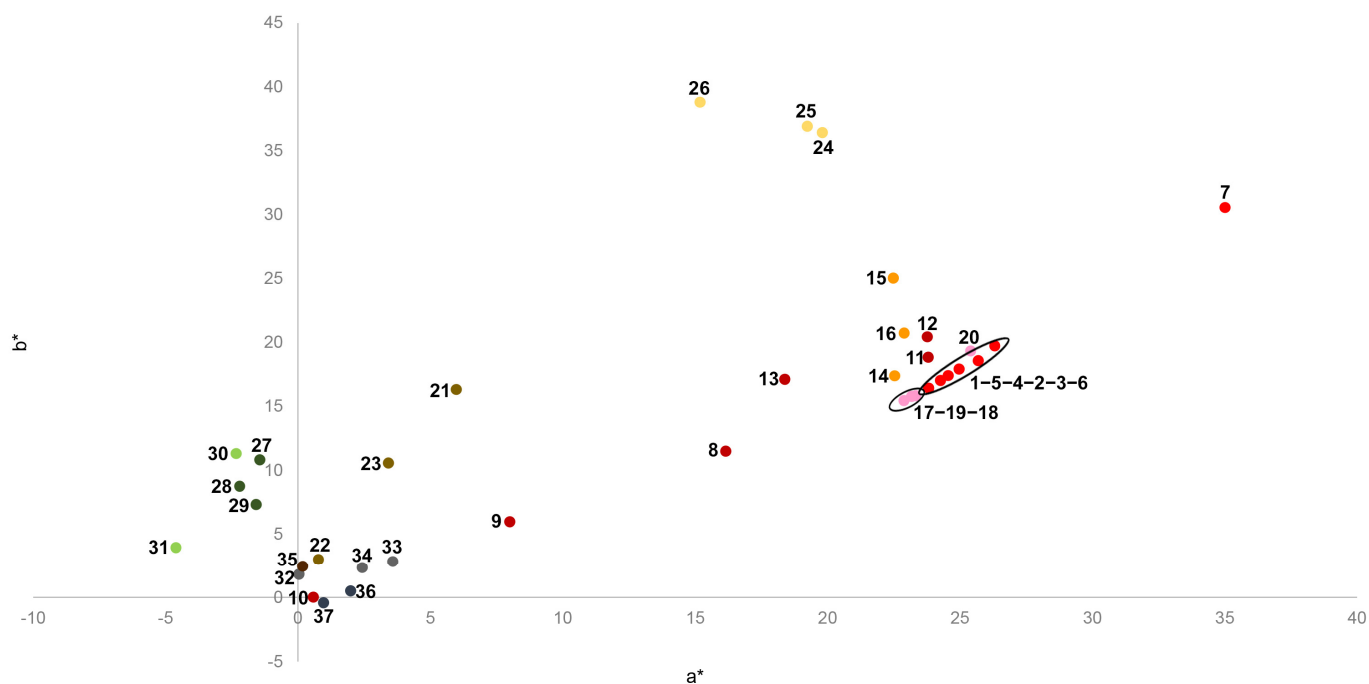
Figure 6. Biplot of a* and b* values of CIEL*a*b* coordinates measured on mixtures replicas. Point colors correspond to the chromatic appearance of replicas (1: MR1; 2: MR2a; 3: MR2b; 4: MR2c; 5: MR3a; 6: MR3b; 7: MR3c; 8: MR4a; 9: MR4b; 10: MR4c; 11: MR5a; 12: MR5b; 13: MR5c; 14: MR6a; 15: MR6b; 16: MR6c; 17: MR7a; 18: MR7b; 19: MR7c; 20: MR8; 21: MY1a; 22: MY1b; 23: MY1c; 24: MY2a; 25: MY2b; 26: MY2c; 27: MG1a; 28: MG1b; 29: MG1c; 30: MG2; 31; MG3; 32: MBG1; 33: MBG2; 34: MBG3; 35: MB1; 36: MB2; 37:MB3).
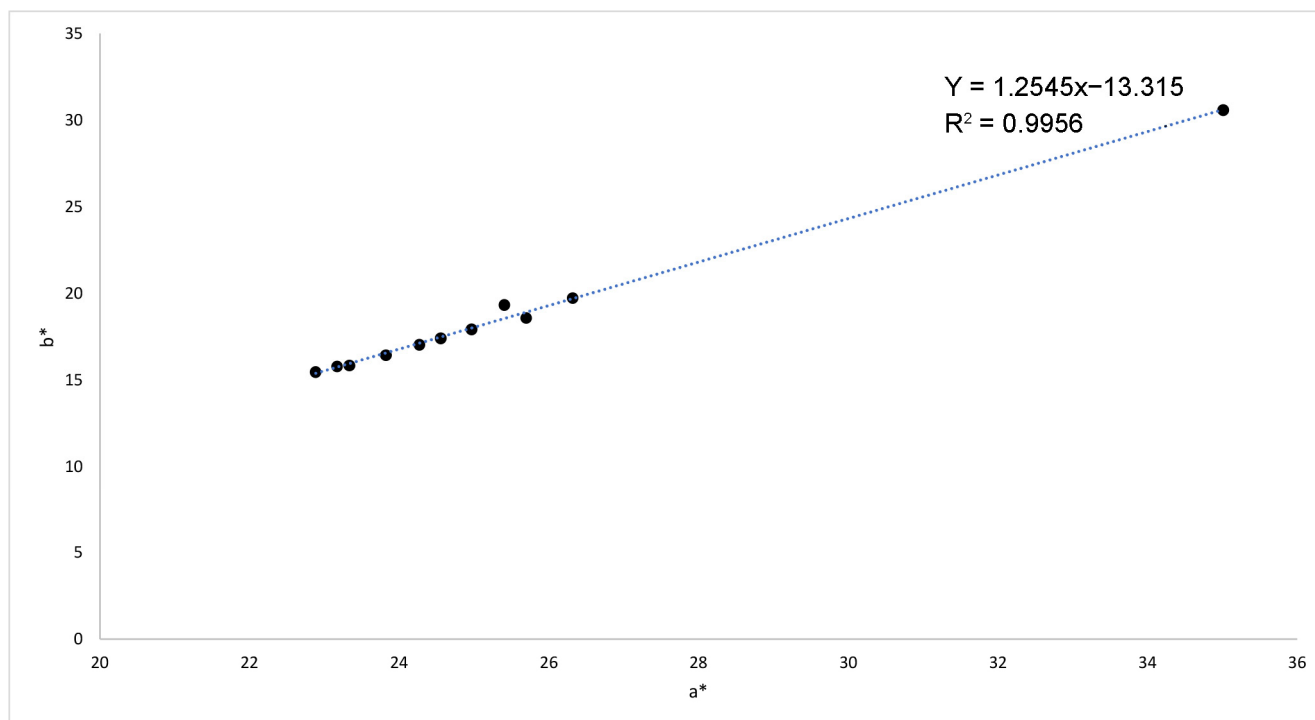

Figure 7. Biplot of a* and b* values of CIEL*a*b* coordinates in mixtures containing hematite. Corresponding points showed a very good ($R^2 = 0.99$) linear correlation.

Table 5. FORS spectral features of pigments (pigments without significant spectral fingerprint were not reported).

Pigment	Sample	FORS Spectral Features
Hematite	P01	~750 nm (max)
Red ochre	P02	~750 nm (max); absorption after ~800 nm
Minium	P03	~560 nm (i.p.); reflectance increasing from ~535 nm
Cinnabar	P04	~600 nm (i.p.); reflectance increasing from ~570 nm
Realgar	P05	~580 nm (max); sharp positive slope between 500 and 600 nm
Yellow ochre	P06	~770 nm (max)
Massicot	P07	~525 nm (i.p.); reflectance increasing from ~420 nm
Green earth	P08	~570 nm (max); ~810 nm (max)
Malachite	P09	~545 nm (max); 600–900 nm (absorbance band)
Verdigris	P10	~480 nm (max); 510–900 (absorbance band)
Azurite	P11	~625 nm (min)
Egyptian blue	P12	~450 nm (max); ~635 nm (min.); ~800 nm (min); ~360 nm (i.p.)
Lapis lazuli	P13	~450 nm (max); ~600 nm (min.); ~700 nm (i.p.)

Concerning red pigments, reflectance spectra of P01 (hematite) and P02 (red ochre) were very similar to each other and displayed a distinctive S-shape and a maximum reflectance centered at 750 nm, according to [10] except for absorption after 800 nm due to the presence in red ochre of other impurities naturally present inside the pigment (i.e., gypsum, clay minerals and feldspars), as also proved by XRPD results.

Differently, the P04 sample (cinnabar) was characterized by a rapid increase in reflectance intensity starting from about 570 nm and an inflection point at ~600 nm, as observed by [58].

Even if previously brown earth (P14) was identified as a brown pigment, the chromatic effect of color in frescos painting was a dark red; then it is compared with the other red samples. The spectrum does not show strong features that allow us to distinguish it from red ochre.

For the same previous reason, samples P03 (minium) and P05 (realgar) were classified as orange pigments. In the first, the spectrum appeared very similar to that of cinnabar, showing a sudden increase in reflectance in the yellow regions, starting from ~535 nm, with a different inflection point around ~560 nm. The realgar instead has a sharp positive slope at the wavelengths between 500 and 600 nm, a maximum near 850 nm.

Referring to yellow pigments, the reflectance curve of P06 (yellow ochre) was similar to the S-shaped spectrum of red ochre and showed a reflectance maximum centered at 770 nm. In sample P07 (massicot) instead, results revealed a different curve with a rapid increase in reflectance intensity starting from about 420 nm and an inflection point at ~525 nm.

As for green coloration, sample P08 (green earth) was marked by two reflectance bands centered at 570 and 810 nm, respectively, according to [10], whereas in the P09 sample (malachite), the curve was marked by a reflectance maximum centered at about 545 nm and a wide absorbance band interesting the region between 600 and 900 nm. Sample P10 (verdigris), early classified as green, showed a reflectance band at ~480 nm and a wide absorbance between 510 and 900 nm.
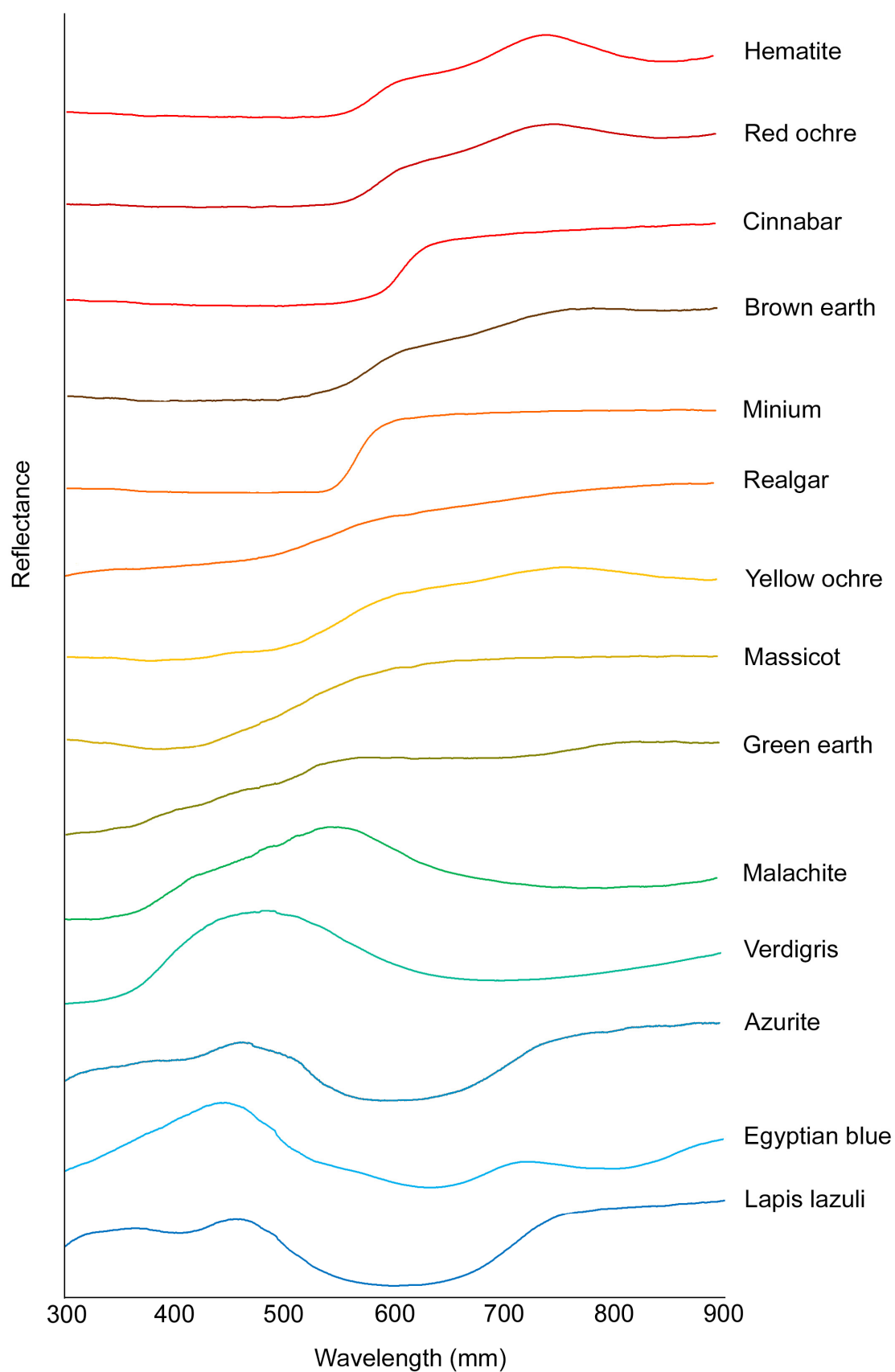
Figure 8. FORS reflectance spectra for the investigated pigments (except for blacks and white).

The trends of blue pigment spectra were very different. The reflectance of sample P11 (azurite) is very low because of the blackening in progress; however, an absorbance band is visible around 625 nm. For samples P12 (Egyptian blue) and P13 (lapis lazuli), results highlighted a reflectance band at 450 nm, even if in Egyptian blue, two absorbance bands were centered at 635 and 800 nm, respectively, whereas in lapis lazuli, spectrum showed an absorbance band shifted at around 600 nm and an inflection point at ~700.

As expected, spectra of bone black (P15), vine black (P16), ivory black (P17) and bianco San Giovanni (P18) were mostly flat.

4.4.2. Mixtures Replicas

The interpretation of FORS replicas revealed interesting results, in particular, on some mixtures. Concerning the MR3 group (hematite and minium), in samples with minium content greater than 75%, it was observed that the S-shaped spectrum (Figure 9a) of the hematite undergoes a variation with an inflection point at ~560 nm, diagnostic of the presence of the minium. For the reflectance spectrum of MR6 group samples, composed of red ochre and yellow ochre, a shift of the absorption band towards higher wavelengths (560 nm) due to the presence of yellow ochre was highlighted. The same occurred in the MR8 sample in which hematite (30%) and yellow ochre (20%) were mixed together with bianco San Giovanni (50%).
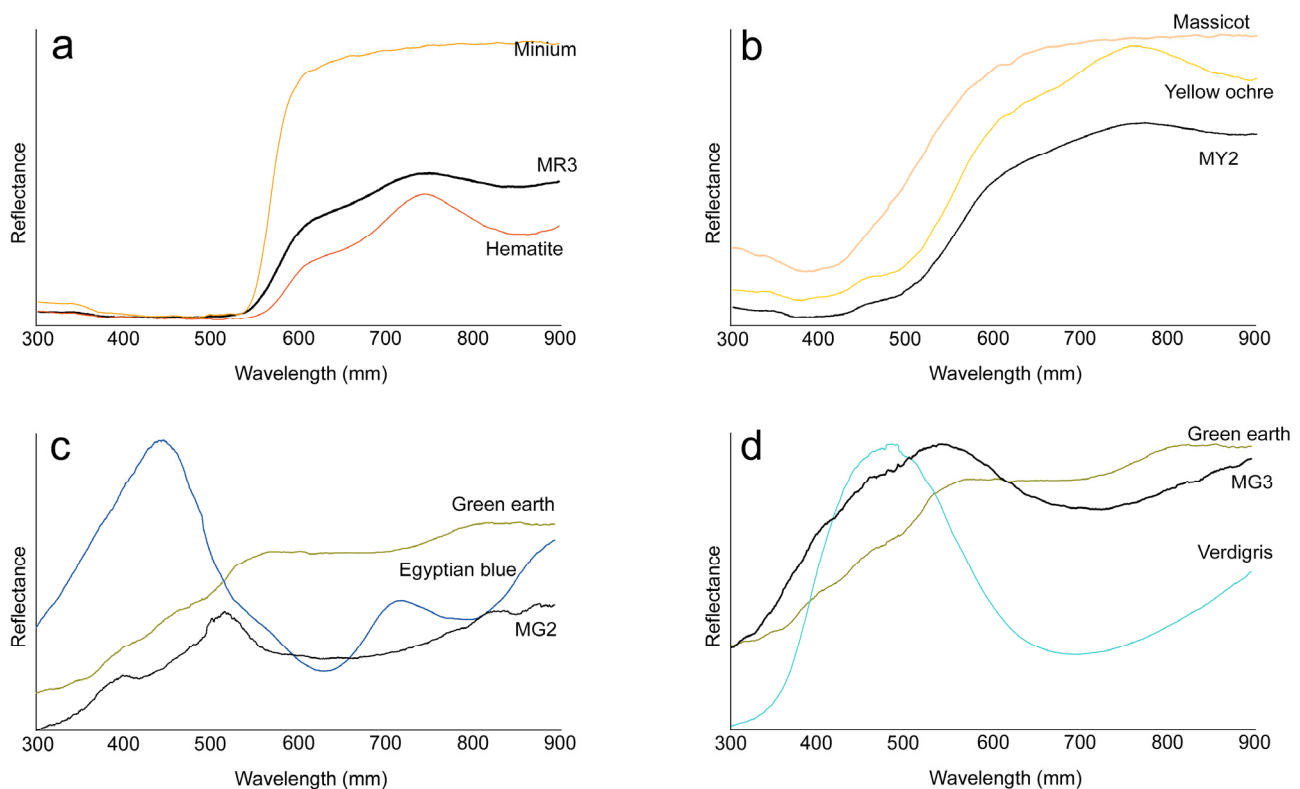

Figure 9. FORS reflectance for some significant mixtures replicas compared with corresponding pigments: MR3 (**a**), MY2 (**b**), MG2 (**c**) and MG3 (**d**).

In the mixtures based on yellow ochre and massicot (MY2), the curve (Figure 9b) showed a maximum reflectance at 770 nm, indicative of yellow ochre, which attenuated as its amount decreased. Similarly, the inflection point at ~525 nm of the massicot was visible and appeared clearer in the MY2c sample.

The MG2 mix showed a spectrum (Figure 9c) similar to that of green earth with an absorption band centered at ~635 nm, indicative of the presence of Egyptian blue. Likewise, in the MG3 sample, the spectrum (Figure 9d) followed the trend of green earth but with a wide absorption band between 550 and 900, a typical marker of verdigris.

Less significant information was obtained from the interpretation of the other mixtures spectra. In particular, in the MR1 sample containing hematite, minium, cinnabar and realgar, the spectrum followed the curve of hematite (70%), while the features of the other components are not visible. A comparable behavior displayed spectra of MR2 group samples, in which hematite and red ochre are mixed. In mixtures composed of vine black and red ochre, only in the sample with an ochre percentage higher than 75% (MR4a) is it possible to appreciate the S-shape and the maximum reflectance centered at 750 nm of the red ochre. In mixtures composed of red ochre and brown earth (MR5), no diagnostic features are observed since the two spectra are comparable. Furthermore, samples with predominant black pigments (MY1, MBG1, MBG2, MBG3, MB1, MB2, MB3) showed an almost flat spectrum where the spectral features of the other pigments were obliterated.

4.5. Key Points

The results obtained by means of the portable digital microscope highlighted distinguishable peculiar features for both pure pigments and pigments' mixtures, which can be used for their identification. They can be summarized as follows:

- Generally, ochres and earths are very recognizable pigments owing to their opaque aspect, rounded shape, low saturation and low brightness of color, size distribution;
- Cinnabar is clearly recognizable for its angular shape and very thick edge, as well as the particular red-magenta color;
- Fine pigments such as, in this research, minium and hematite are certainly more difficult to identify because the morphological features of particles are not observable to the microscope magnification. However, even if it cannot be considered a distinctive parameter, certainly the visible color suggests preliminary information to hypothesize under the microscope and verified by other analytical techniques, i.e., FORS;
- Malachite and azurite are recognizable because they both show a typical color and a fractured appearance;
- Verdigris is identifiable because it includes acicular cyan particles with high saturation and brightness;
- Egyptian blue and lapis lazuli were similar but different in color and shape, which is typically tabular in lapis lazuli;
- Bianco San Giovanni shows large and spherical particles;
- Among the black pigments, the vine black is clearly revealable because consists of a tabular particle with high gloss;
- As a rule, the microscopic identification seems to be easier for blue and green colors and for mixtures that contain contrasting colors (i.e., hematite and bianco San Giovanni, red ochre and vine black, yellow ochre and vine black);
- In mixing composed of vine black and very limited amounts of red or yellow ochres (a recipe widespread in the Apulia wall painting to realize differently shaded black), which appeared black to the naked eye, the identification of all the pigment within is feasible. Conversely, mixtures including similar (in terms of color) pigments, such as hematite and red ochre, red ochre and brown earth, and yellow ochre and massicot, are obviously unrecognizable.
- Concerning the colorimetric data, results indicated the following:
- Very noteworthy is the linear positive correlation of a* and b* values in all mixtures including hematite.
- Acquiring and interpreting FORS spectra revealed the following significant aspects:
- The comparison between mixtures and pure pigments allowed a better understanding of the light reflection and scattering phenomena that occur when a mix of pigments is present;
- All pigments can be easily detected by the presence of absorption bands, inflection points, or other diagnostic spectral features. The exceptions are black and white pigments, where the spectrum is a nearly flat curve;
- Pigments having a very similar curve, but which nonetheless allow the identification, are ochres (red and yellow) and brown earth;

- Green pigments, although having comparable spectra, can be clearly identified by the presence of more or less large absorption bands centered at different wavelengths;
- Blue pigments show very different and characteristic reflectance spectra, therefore in this case, their identification is rather simplified;
- The type of binder used (water or lime) has no influence on the spectral features since the lime-based plaster incorporates the pigment similarly in the case of fresco and *mezzo fresco* painting, also because the chemical composition of the involved materials (plaster and lime as a binder) is the same. This analogy cannot be definitely extended to the other binders used in painting as well;
- The analysis of mixtures containing pigments with similar reflectance spectra (red ochre + yellow ochre, red ochre + hematite, red ochre + brown earth) is rather difficult;
- In mixtures containing more than 75% of black pigments, the contribution of the latter hides the spectral features of the other pigments;
- The presence of inflection points could allow the identification of corresponding pigments even in more complex mixtures, for example in those containing yellow ochre and massicot.

5. Conclusions

The non-invasive methodology proposed in this research brings together the results of the analysis on pictorial surfaces, comparing observations by a portable digital microscope, measurement of color coordinates and interpretation of reflectance spectra acquired by FORS in order to identify the composition of pure pigments and their mixtures.

For test validation, replicas of wall paintings were reproduced using pigments and mixtures of pigments, which were very recurrent in Apulia, but which were frequently used for wall paintings overall.

The presented dataset showed that on the basis of microscopic distinctive parameters, color coordinates and reflectance spectra, the identification of pigments is feasible. On the other hand, very significant is the complementarity of results obtained by FORS and microscopic observations, both on pure pigments and mixtures: pigments clearly visible under the portable microscope (i.e., cinnabar in a mixture composed of other red pigments and very few amounts of ochres in a black mixture) cannot be detected by FORS and, conversely, mixtures such as that composed by yellow ochre and massicot cannot be characterized by microscope even if their spectral features recorder by FORS are diagnostic of each pigment.

All the results obtained in this study constitute a database, which can be easily consulted as a comparison tool in the characterization of the pictorial wall surfaces of Apulia artistic and archaeological contexts. In this regard, one of the most interesting future prospects is the application of the presented approach on (historical and modern) pigments used in historical-artistic sites and then the comparison between the results obtained in situ and those observed on the replicas. In this sense, a first application work is being completed and submitted. Furthermore, since pigments and the mixture considered in this study are frequent even outside the region, the library can certainly represent a reference dataset also for other national and international case studies.

Supplementary Materials: The following supporting information can be downloaded at: https://www.mdpi.com/article/10.3390/heritage6020084/s1, Figure S1. Photomicrograph of P01 (*hematite*); Figure S2. Photomicrograph of P02 (*red ochre*); Figure S3. Photomicrograph of P03 (*minium*); Figure S4. Photomicrograph of P04 (*cinnabar*); Figure S5. Photomicrograph of P05 (*realgar*); Figure S6. Photomicrograph of P06 (*yellow ochre*); Figure S7. Photomicrograph of P07 (*massicot*); Figure S8. Photomicrograph of P08 (*green earth*); Figure S9. Photomicrograph of P09 (*malachite*); Figure S10. Photomicrograph of P10 (*verdigris*); Figure S11. Photomicrograph of P11 (*azurite*); Figure S12. Photomicrograph of P12 (*egyptian blue*); Figure S13. Photomicrograph of P13 (*lapis lazuli*); Figure S14. Photomicrograph of P14 (*brown earth*); Figure S15. Photomicrograph of P15 (*bone black*); Figure S16. Photomicrograph of P16 (*vine black*); Figure S17. Photomicrograph of P17 (*ivory black*); Table S1. L*, a* and b* mean values and standard

deviation of each pigment applied by frescos and lime painting techniques; Table S2. L*, a* and b* mean values and standard deviation of mixing.

References

1. Galli, A.; Caccia, M.; Bonizzoni, L.; Gargano, M.; Ludwig, N.; Poldi, G.; Martini, M. Deep inside the Color: How Optical Microscopy Contributes to the Elemental Characterization of a Painting. *Microchem. J.* **2020**, *155*, 104730. [CrossRef]
2. Corradini, M.; de Ferri, L.; Pojana, G. Fiber Optic Reflection Spectroscopy–Near-Infrared Characterization Study of Dry Pigments for Pictorial Retouching. *Appl. Spectrosc.* **2021**, *75*, 445–461. [CrossRef] [PubMed]
3. Delaney, J.K.; Ricciardi, P.; Glinsman, L.D.; Facini, M.; Thoury, M.; Palmer, M.; de la Rie, E.R. Use of Imaging Spectroscopy, Fiber Optic Reflectance Spectroscopy, and X-Ray Fluorescence to Map and Identify Pigments in Illuminated Manuscripts. *Stud. Conserv.* **2014**, *59*, 91–101. [CrossRef]
4. Raicu, T.; Zollo, F.; Falchi, L.; Barisoni, E.; Piccolo, M.; Izzo, F.C. Preliminary Identification of Mixtures of Pigments Using the paletteR Package in R—The Case of Six Paintings by Andreina Rosa (1924–2019) from the International Gallery of Modern Art Ca' Pesaro, Venice. *Heritage* **2023**, *6*, 524–547. [CrossRef]
5. Piccolo, A.; Bonato, E.; Falchi, L.; Lucero-Gómez, P.; Barisoni, E.; Piccolo, M.; Balliana, E.; Cimino, D.; Izzo, F.C. A Comprehensive and Systematic Diagnostic Campaign for a New Acquisition of Contemporary Art—The Case of Natura Morta by Andreina Rosa (1924–2019) at the International Gallery of Modern Art Ca' Pesaro, Venice. *Heritage* **2021**, *4*, 4372–4398. [CrossRef]
6. Krämer, M.; Henniges, U.; Brückle, I.; Lenfant, L.; Drüppel, K. Analysis of Red Chalk Drawings from the Workshop of Giovanni Battista Piranesi Using Fiber Optics Reflectance Spectroscopy. *Herit. Sci.* **2021**, *9*, 112. [CrossRef]
7. Zaleski, S.; Montagnino, E.; Brostoff, L.; Muller, I.; Buechele, A.; Lynn Ward-Bamford, C.; France, F.; Loew, M. Application of Fiber Optic Reflectance Spectroscopy for the Detection of Historical Glass Deterioration. *J. Am. Ceram. Soc.* **2020**, *103*, 158–166. [CrossRef]
8. Gulmini, M.; Idone, A.; Diana, E.; Gastaldi, D.; Vaudan, D.; Aceto, M. Identification of Dyestuffs in Historical Textiles: Strong and Weak Points of a Non-Invasive Approach. *Dyes Pigm.* **2013**, *98*, 136–145. [CrossRef]
9. Bacci, M.; Baldini, F.; Carlà, R.; Linari, R. A Color Analysis of the Brancacci Chapel Frescoes. *Appl. Spectrosc.* **1991**, *45*, 26–31. [CrossRef]
10. Cheilakou, E.; Troullinos, M.; Koui, M. Identification of Pigments on Byzantine Wall Paintings from Crete (14th Century AD) Using Non-Invasive Fiber Optics Diffuse Reflectance Spectroscopy (FORS). *J. Archaeol. Sci.* **2014**, *41*, 541–555. [CrossRef]
11. Pagano, S.; Germinario, C.; Alberghina, M.F.; Covolan, M.; Mercurio, M.; Musmeci, D.; Piovesan, R.; Santoriello, A.; Schiavone, S.; Grifa, C. Multilayer Technology of Decorated Plasters from the Domus of Marcus Vipsanus Primigenius at Abellinum (Campania Region, Southern Italy): An Analytical Approach. *Minerals* **2022**, *12*, 1487. [CrossRef]
12. Picollo, M.; Bacci, M.; Casini, A.; Lotti, F.; Porcinai, S.; Radicati, B.; Stefani, L. Fiber Optics Reflectance Spectroscopy: A Non-Destructive Technique for the Analysis of Works of Art. In *Optical Sensors and Microsystems*; Martellucci, S., Chester, A.N., Mignani, A.G., Eds.; Kluwer Academic Publishers: Boston, MA, USA, 2002; pp. 259–265. [CrossRef]
13. Cosentino, A. FORS Spectral Database of Historical Pigments in Different Binders. *e-cons* **2014**, *2*, 54–65. [CrossRef]
14. Dupuis, G.; Elias, M.; Simonot, L. Pigment Identification by Fiber-Optics Diffuse Reflectance Spectroscopy. *Appl. Spectrosc.* **2002**, *56*, 1329–1336. [CrossRef]
15. Liang, H.; Saunders, D.; Cupitt, J.A. A new multispectral imaging system for examining paintings. *J. Imaging Sci. Technol.* **2005**, *49*, 551–562.

16. Bonizzoni, L.; Caglio, S.; Galli, A.; Poldi, G. A non invasive method to detect stratigraphy, thicknesses and pigment concentration of pictorial multilayers based on EDXRF and vis-RS: In situ applications. *Appl. Phys. A* **2008**, *92*, 203–210. [CrossRef]

17. Pozo-Antonio, J.S.; Cardell, C.; Sánchez, S.; Montes Rueda, J. Reflectance of Oil Paintings: Influence of Paint Layer Thickness and Binder Amount. *Coatings* **2022**, *12*, 601. [CrossRef]

18. Cavaleri, T.; Giovagnoli, A.; Nervo, M. Pigments and Mixtures Identification by Visible Reflectance Spectroscopy. *Procedia Chem.* **2013**, *8*, 45–54. [CrossRef]

19. Elias, M.; Chartier, C.; Prévot, G.; Garay, H.; Vignaud, C. The Colour of Ochres Explained by Their Composition. Mater. *Sci. Eng. B* **2006**, *127*, 70–80. [CrossRef]

20. Miriello, D.; Bloise, A.; Crisci, G.; De Luca, R.; De Nigris, B.; Martellone, A.; Osanna, M.; Pace, R.; Pecci, A.; Ruggieri, N. Non-Destructive Multi-Analytical Approach to Study the Pigments of Wall Painting Fragments Reused in Mortars from the Archaeological Site of Pompeii (Italy). *Minerals* **2018**, *8*, 134. [CrossRef]

21. Lorusso, S.; Natali, A.; Matteucci, C. Colorimetry Applied to the Field of Cultural Heritage: Examples of Study Cases. *Conserv. Sci. Cult. Herit.* **2007**, *7*, 187–220. [CrossRef]

22. Villafana, T.; Edwards, G. Creation and Reference Characterization of Edo Period Japanese Woodblock Printing Ink Colorant Samples Using Multimodal Imaging and Reflectance Spectroscopy. *Herit. Sci.* **2019**, *7*, 94. [CrossRef]

23. Pinto, D.; Laviano, R.; Bianchi, V. Archaeometric Investigations on Wall Paintings from the Hypogeum of S. Marco (Fasano - Brindisi, Southern Italy). *Plinius* **2008**, *34*, 348.

24. Capitanio, D.; Laviano, R.; Menga, A.; Meo-Evoli, N.; Vona, F.; Vurro, F. Intonaci e Pitture Murali Dell'ipogeo Di S. Matteo All'Arena, Monopoli (Bari). In Proceedings of the Sulle Pitture Murali, Conference Scienza e Beni Culturali (XXI), Bressanone, Italy, 12–15 July 2005; Arcadia Ricerche ed: Marghera-Venezia, Italy, 2005; pp. 1137–1146.

25. Fioretti, G.; Garavelli, A.; Germinario, G.; Pinto, D. Archaeometric Study of Wall Rock Paintings from the Sant'Angelo in Criptis Cave, Santeramo in Colle, Bari: Insights on the Rupestrian Decorative Art in Apulia (Southern Italy). *Archaeol. Anthropol. Sci.* **2021**, *13*, 168. [CrossRef]

26. Calia, A.; Giorgi, M.; Quarta, G.; Masieri, M. Le pitture della cripta del Gonfalone a Tricase (Lecce): Problematiche storico-artistiche e contributo alla identificazione dei pigmenti attraverso FRX portatile. In Proceedings of the Conference BENI Culturali in Puglia Dialoghi Multidisciplinari per la Ricerca, la Tutela e la Valorizzazione, Bari, Italy, 16–17 September 2020; Fioretti, G., Ed.; Edizioni Fondazione Pasquale Battista: Milano, Italy, 2021; pp. 125–132.

27. Fioretti, G.; Raneri, S.; Pinto, D.; Mignozzi, M.; Mauro, D. The Archaeological Site of St. Maria Veterana (Triggiano, Southern Italy): Archaeometric Study of the Wall Paintings for the Historical Reconstruction. *J. Archaeol. Sci. Rep.* **2020**, *29*, 102080. [CrossRef]

28. Calia, A.; Melica, D.; Quarta, G. I Dipinti Murali Del Tempietto: Materiali Costituenti e Tecniche Esecutive. In *Masseria Seppannibale Grande in agro di Fasano (BR)*; Bertelli, G., Lepore, G., Eds.; Adda: Bari, Italy, 2011; pp. 195–206.

29. Pinto, D. Analisi Di Alcuni Campioni Di Intonaco Dipinto Della Cupola Orientale. In *Masseria Seppannibale Grande in agro di Fasano (BR)*; Bertelli, G., Lepore, G., Eds.; Adda: Bari, Italy, 2011; pp. 207–209.

30. De Benedetto, G.E.; Fico, D.; Margapoti, E.; Pennetta, A.; Cassiano, A.; Minerva, B. The Study of the Mural Painting in the 12th Century Monastery of Santa Maria Delle Cerrate (Puglia-Italy): Characterization of Materials and Techniques Used: Study of Painting at the Santa Maria Delle Cerrate Church. *J. Raman Spectrosc.* **2013**, *44*, 899–904. [CrossRef]

31. Fico, D.; Pennetta, A.; Rella, G.; Savino, A.; Terlizzi, V.; De Benedetto, G.E. A Combined Analytical Approach Applied to Medieval Wall Paintings from Puglia (Italy): The Study of Painting Techniques and Its Conservation State: Study of Painting Techniques and Its Conservation State. *J. Raman Spectrosc.* **2016**, *47*, 321–328. [CrossRef]

32. Calia, A.; Giannotta, M.T. La tomba dei Festoni in via Crispi a Taranto: Individuazione e riconoscimento dei pigmenti utilizzati nelle pitture. In Proceedings of the III Congresso Nazionale di Archeometria, Bressanone, Italy, 13–14 February 2004; D'amico, C., Ed.; Pàtron: Bologna, Italy, 2005; pp. 271–278.

33. Frezzato, F. Cennino Cennini. In *IL Libro Dell'Arte*; Neri Pozza: Vicenza, Italy, 2009.

34. Piovesan, R.; Mazzoli, C.; Maritan, L.; Cornale, P. Fresco and Lime-Paint: An Experimental Study and Objective Criteria for Distinguishing between These Painting Techniques: Distinguishing between Fresco and Lime-Paint. *Archaeometry* **2012**, *54*, 723–736. [CrossRef]

35. Regazzoni, L.; Cavallo, G.; Biondelli, D.; Gilardi, J. Microscopic Analysis of Wall Painting Techniques: Laboratory Replicas and Romanesque Case Studies in Southern Switzerland. *Stud. Conserv.* **2018**, *63*, 326–341. [CrossRef]

36. McLaren, K. XIII—The development of the CIE 1976 (L* a* b*) uniform colour space and colour difference formula. *J. Soc. Dye Colour* **1976**, *92*, 338–341. [CrossRef]

37. Menges, F. Spectragryph-Optical Spectroscopy Software, Version 1.2.16; Oberstdorf, Germany. 2022. Available online: https://www.effemm2.de/spectragryph/ (accessed on 30 June 2022).

38. Mastrotheodoros, G.P.; Beltsios, K.G. Pigments—Iron-Based Red, Yellow, and Brown Ochres. *Archaeol. Anthropol. Sci.* **2022**, *14*, 35. [CrossRef]

39. Gliozzo, E.; Burgio, L. Pigments—Arsenic-Based Yellows and Reds. *Archaeol. Anthropol. Sci.* **2022**, *14*, 4. [CrossRef]

40. Cáceres-Rivero, C.; Tupa-Quispe, A.L.; Torres-Casas, R.; Bedregal, P. Identification of adulterants in artistic earth pigments using a multi-technique approach. *Results Chem.* **2022**, *4*, 100561. [CrossRef]

41. Cardell, C.; Herrera, A.; Guerra, I.; Navas, N.; Rodríguez Simón, L.; Elert, K. Pigment-size effect on the physico-chemical behavior of azurite-tempera dosimeters upon natural and accelerated photo aging. *Dyes Pigm.* **2017**, *141*, 53–65. [CrossRef]

42. Schmidt Patterson, C.; Walton, M.; Trentelman, K. Characterization of Lapis Lazuli Pigments Using a Multitechnique Analytical Approach: Implications for Identification and Geological Provenancing. *Anal. Chem.* **2009**, *81*, 8513–8518. [CrossRef]

43. González-Cabrera, M.; Arjonilla, P.; Domínguez-Vidal, A.; Ayora-Cañada, M.J. Natural or synthetic? Simultaneous Raman/luminescence hyperspectral microimaging for the fast distinction of ultramarine pigments. *Dyes Pigm.* **2020**, *178*, 108349. [CrossRef]

44. Van Loon, A.; Boon, J.J. Characterization of the deterioration of bone black in the 17th century Oranjezaal paintings using electron-microscopic and micro-spectroscopic imaging techniques. *Spectrochim. Acta Part B At. Spectrosc.* **2004**, *59*, 1601–1609. [CrossRef]

45. Elert, K.; Herrera, A.; Cardell, C. Pigment-binder interactions in calcium-based tempera paints. *Dyes Pigm.* **2018**, *148*, 236–248. [CrossRef]

46. Hradil, D.; Grygar, T.; Hradilová, J.; Bezdička, P. Clay and Iron Oxide Pigments in the History of Painting. *Appl. Clay Sci.* **2003**, *22*, 223–236. [CrossRef]

47. Cotte, M.; Susini, J.; Metrich, N.; Moscato, A.; Gratziu, C.; Bertagnini, A.; Pagano, M. Blackening of Pompeian Cinnabar Paintings: X-Ray Microspectroscopy Analysis. *Anal. Chem.* **2006**, *78*, 7484–7492. [CrossRef]

48. Miguel, C.; Pinto, J.V.; Clarke, M.; Melo, M.J. The Alchemy of Red Mercury Sulphide: The Production of Vermilion for Medieval Art. *Dyes Pigm.* **2014**, *102*, 210–217. [CrossRef]

49. Gliozzo, E. Pigments—Mercury-Based Red (Cinnabar-Vermilion) and White (Calomel) and Their Degradation Products. *Archaeol. Anthropol. Sci.* **2021**, *13*, 210. [CrossRef]

50. Gliozzo, E.; Ionescu, C. Pigments—Lead-Based Whites, Reds, Yellows and Oranges and Their Alteration Phases. *Archaeol. Anthropol. Sci.* **2022**, *14*, 17. [CrossRef]

51. Keune, K.; Mass, J.; Mehta, A.; Church, J.; Meirer, F. Analytical Imaging Studies of the Migration of Degraded Orpiment, Realgar, and Emerald Green Pigments in Historic Paintings and Related Conservation Issues. *Herit. Sci.* **2016**, *4*, 10. [CrossRef]

52. Kotulanová, E.; Bezdička, P.; Hradil, D.; Hradilová, J.; Švarcová, S.; Grygar, T. Degradation of Lead-Based Pigments by Salt Solutions. *J. Cult. Herit.* **2009**, *10*, 367–378. [CrossRef]

53. Švarcová, S.; Hradil, D.; Hradilová, J.; Čermáková, Z. Pigments—Copper-Based Greens and Blues. *Archaeol. Anthropol. Sci.* **2021**, *13*, 190. [CrossRef]

54. Favaro, M.; Guastoni, A.; Marini, F.; Bianchin, S.; Gambirasi, A. Characterization of Lapis Lazuli and Corresponding Purified Pigments for a Provenance Study of Ultramarine Pigments Used in Works of Art. *Anal. Bioanal. Chem.* **2012**, *402*, 2195–2208. [CrossRef]

55. Salvadó, N.; Butí, S.; Aranda MA, G.; Pradell, T. New Insights on Blue Pigments Used in 15th Century Paintings by Synchrotron Radiation-Based Micro-FTIR and XRD. *Anal. Methods* **2014**, *6*, 3610. [CrossRef]

56. Ganio, M.; Pouyet, E.S.; Webb, S.M.; Schmidt Patterson, C.M.; Walton, M.S. From Lapis Lazuli to Ultramarine Blue: Investigating Cennino Cennini's Recipe Using Sulfur K-Edge XANES. *Pure Appl. Chem.* **2018**, *90*, 463–475. [CrossRef]

57. Tomasini, E.; Siracusano, G.; Maier, M.S. Spectroscopic, Morphological and Chemical Characterization of Historic Pigments Based on Carbon. Paths for the Identification of an Artistic Pigment. *Microchem. J.* **2012**, *102*, 28–37. [CrossRef]

58. Clark, R.N. Reflectance Spectra. In *Rock Physics and Phase Relations: A Handbook of Physical Constants*; Ahrens, T.J., Ed.; American Geophysical Union: Washington, DC, USA, 1995; Volume 3, pp. 178–188.